10-16-2009

Giant Plasmonic Energy and Momentum Transfer on the Nanoscale

Maxim Durach
Georgia State University

GIANT PLASMONIC ENERGY AND MOMENTUM TRANSFER ON THE NANOSCALE

by

MAXIM DURACH

Under the Direction of Dr. Mark I. Stockman

ABSTRACT

We have developed a general theory of the plasmonic enhancement of many-body phenomena resulting in a closed expression for the surface plasmon-dressed Coulomb interaction. It is shown that this interaction has a resonant nature. We have also demonstrated that renormalized interaction is a long-ranged interaction whose intensity is considerably increased compared to bare Coulomb interaction over the entire region near the plasmonic nanostructure. We illustrate this theory by re-deriving the mirror charge potential near a metal sphere as well as the quasistatic potential behind the so-called perfect lens at the surface plasmon (SP) frequency. The dressed interaction for an important example of a metal–dielectric nanoshell is also explicitly calculated and analyzed.

The renormalization and plasmonic enhancement of the Coulomb interaction is a universal effect, which affects a wide range of many-body phenomena in the vicinity of metal nanostructures: chemical reactions, scattering between charge carriers, exciton formation, Auger recombination, carrier multiplication, etc. We have described the nanoplasmonic-enhanced Förster resonant energy transfer (FRET) between quantum dots near a metal nanoshell. It is shown that this process is very efficient near high-aspect-ratio nanoshells.

We have also obtained a general expression for the force exerted by an electromagnetic field on an extended polarizable object. This expression is applicable to a wide range of situations important for nanotechnology. Most importantly, this result is of fundamental importance for processes involving interaction of nanoplasmonic fields with metal electrons.

Using the obtained expression for the force, we have described a giant surface-plasmon-induced drag-effect rectification (SPIDER), which exists under conditions of the extreme nanoplasmonic confinement. Under realistic conditions in nanowires, this giant SPIDER generates rectified THz potential differences up to $10\,\mathrm{V}$ and extremely strong electric fields up to $10^5 - 10^6\,\mathrm{V/cm}$. It can serve as a powerful nanoscale source of THz radiation. The giant SPIDER opens up a new field of ultraintense THz nanooptics with wide potential applications in nanotechnology and nanoscience, including microelectronics, nanoplasmonics, and biomedicine. Additionally, the SPIDER is an ultrafast effect whose bandwidth for nanometric wires is 20 THz, which allows for detection of femtosecond pulses on the nanoscale.

INDEX WORDS: Nanoplasmonics, Nanoplasmonic renormalization of Coulomb interaction, Surface-plasmon enhanced Förster energy transfer (FRET), Surface-plasmon-induced drag-effect rectification (SPIDER), Nanotechnology, Plasmonics on the nanoscale, Localized surface plasmons (LSPs), Surface plasmon polaritons (SPPs)

GIANT PLASMONIC ENERGY AND MOMENTUM TRANSFER ON THE NANOSCALE

by

MAXIM DURACH

A Dissertation Submitted in Partial Fulfillment of the Requirements for the Degree of

Doctor of Philosophy

in the College of Arts and Sciences

Georgia State University

2009

GIANT PLASMONIC ENERGY AND MOMENTUM TRANSFER ON THE NANOSCALE

by

MAXIM DURACH

Committee Chair: Dr. Mark Stockman

Committee: Dr. Vadym Apalkov

Dr. Nikolaus Dietz

Dr. Steven Manson

Dr. Unil Perera

Dr. Paul Wiita

Electronic Version Approved:

Office of Graduate Studies

College of Arts and Sciences

Georgia State University

December 2009

Acknowledgements

First of all, I would like to express gratitude to my adviser Prof. Mark I. Stockman for wonderful, interesting physics problems he proposed, for his guidance, advice and fruitful joint work during the past three years.

I would like to thank the members of my committee, the Chair of the Department, Dr. Richard Miller, and faculty members for enriching classes and a productive atmosphere.

I am thankful to my parents Anna and Eduard Duracz for encouraging me to go to another hemisphere for education. Their daily support was felt across the Atlantic Ocean. Of course, I would like to thank Anastasia Rusina for being with me all this time.

Table of Contents

List of Figures

List of Abbreviations

SP	Surface plasmon
FRET	Förster resonant energy transfer
SPIDER	Surface-Plasmon-Induced Drag Effect Rectification
LSP	Localized Surface Plasmon
SPP	Surface Plasmon Polariton
THz	Terahertz
NQD	Nanocrystal Quantum Dot
SERS	Surface Enhanced Raman Scattering
IR	Infrared

Chapter 1. Quasistatic Approximation and Surface Plasmons (SPs)

1.1 Quasistatic Approximation

The Maxwell equations relate time and space derivatives of the electromagnetic field with charges and currents. In many cases the time variation of fields is not fast enough, and terms with temporal derivatives are overpowered by terms with spatial gradients. In such situations electric and magnetic fields decouple and the electric field is determined only by the charge density $\rho(\mathbf{r},t)$, while the magnetic field arises from currents. Two equations describing the local (microscopic) electric field $\mathbf{e}(\mathbf{r},t)$ under these circumstances are [1-3]:

$$\nabla \cdot \mathbf{e}(\mathbf{r},t) = 4\pi\rho(\mathbf{r},t)\,, \tag{1.1}$$

$$\nabla \times \mathbf{e}(\mathbf{r},t) = 0\,. \tag{1.2}$$

Finding a solution of microscopic equations (1.1) and (1.2) is possible for individual atoms or molecules, but is an extremely complicated many-body problem even for a nanoscopic particle consisting of several atoms. Not only is it very time-consuming to solve microscopic equations (1.1) and (1.2) numerically, it is hard to analyze such a solution or compare it to an experiment, since it contains too many initial parameters, e.g. atomic coordinates, velocities etc. It is much more approachable to obtain a spatially averaged macroscopic field $\mathbf{E} = \bar{\mathbf{e}}$. It differs from the exact microscopic solution $\mathbf{e}(\mathbf{r},t)$ by sharp spatial and temporal field fluctuations $\Delta\mathbf{e} = (\mathbf{e} - \mathbf{E})$ connected with the microscopic composition and dynamics of matter. In the overwhelming majority of practical situations it is enough to know the average macroscopic field

in order to explain the optical phenomena on the macroscale. Nevertheless, fluctuations have been shown to be important on the nanoscale in the studies of non-linear optical effects in rough or fractal metal composites [4, 5]. In this work we will focus on the effects of the average (macroscopic) field, assuming that structures we consider are homogeneous and have smooth enough surfaces to avoid large contributions from fluctuations.

In the charged systems the macroscopic average of the charge density from Eq. (1.1) can be represented using the polarization vector $\mathbf{P}$:

$$\overline{\rho} = \rho_{ext} - \nabla \cdot \mathbf{P}\,, \tag{1.3}$$

where only so-called external charges ρ_{ext} contribute to the total macroscopic charge of a structure [6]. The polarization vector also determines macroscopic surface charge density

$$\overline{\sigma} - \sigma_{ext} = (\mathbf{P} \cdot \hat{\mathbf{n}})\,. \tag{1.4}$$

on the surface of a polarized object, with normal ort $\hat{\mathbf{n}}$ pointing outward. Here σ_{ext} is the surface density of the external charges.

Using Eqs. (1.1)-(1.4), one is able to obtain the equations describing macroscopic electrostatic fields

$$\nabla \cdot \mathbf{D}(\mathbf{r}) = 4\pi\rho_{ext}(\mathbf{r})\,, \tag{1.5}$$

$$\nabla \times \mathbf{E}(\mathbf{r}) = 0\,, \tag{1.6}$$

where the electric induction vector $\mathbf{D} = \mathbf{E} + 4\pi\mathbf{P}$ was introduced. It is easy to notice that Eqs. (1.5)-(1.6) hold not only for time-dependent vector fields $\mathbf{D}(\mathbf{r},t)$ and $\mathbf{E}(\mathbf{r},t)$, but also for their temporal Fourier amplitudes defined by

$$\mathbf{D}(\mathbf{r},\omega) = \int_{-\infty}^{\infty} \mathbf{D}(\mathbf{r},t) e^{i\omega t} dt\,, \tag{1.7}$$

$$\mathbf{E}(\mathbf{r},\omega)=\int_{-\infty}^{\infty}\mathbf{E}(\mathbf{r},t)e^{i\omega t}dt\,. \tag{1.8}$$

On the surface, as it follows from Eqs. (1.5)-(1.6), vectors **D** and **E** should satisfy boundary conditions [2, 6]:

$$(\mathbf{D}_{out}-\mathbf{D}_{in})\cdot\mathbf{n}=4\pi\sigma_{ext} \tag{1.9}$$

$$\mathbf{n}\times(\mathbf{E}_{out}-\mathbf{E}_{in})=0\,. \tag{1.10}$$

To form a full system of equations, Eqs. (1.5)-(1.6) need to be supplemented by the so-called material equation, relating vector fields **D** and **E**. In weak fields this relation is linear. Such a linear dependence can be introduced using the dielectric permittivity $\varepsilon(\mathbf{r},\omega)$:

$$\mathbf{D}(\mathbf{r},\omega)=\varepsilon(\mathbf{r},\omega)\mathbf{E}(\mathbf{r},\omega)\,. \tag{1.11}$$

The relationship (1.11) implies that polarization is determined by the electric field locally and does not depend on the field in the neighboring volumes. This local material equation is a very good approximation for nano-optics until the size of the nanostructure reaches some structural size of the medium [7]. In metals, which hold major significance for this work, nonlocal effects make themselves known when the nanostructure size approaches the plasma correlation length $r_c=v_F/\omega\sim 1\text{nm}$ at optical frequencies, where $v_F\sim 10^8\ \text{cm/s}$ is the Fermi velocity [8-11].

Equation (1.6) means that in quasistatics the macroscopic electric field is conservative and can be expressed as (similarly to the microscopic field **e**, cf. Eq. (1.2))

$$\mathbf{E}(\mathbf{r},\omega)=-\nabla\varphi(\mathbf{r},\omega)\,, \tag{1.12}$$

where the function $\varphi(\mathbf{r},t)$ is the macroscopic electric potential. From equation (1.5) it follows that the potential $\varphi(\mathbf{r},t)$ satisfies the Poisson equation

$$\nabla\left[\varepsilon(\mathbf{r},\omega)\nabla\varphi(\mathbf{r},\omega)\right]=-4\pi\rho_{ext}(\mathbf{r},\omega)\,. \tag{1.13}$$

The boundary conditions (1.9)-(1.10) can be formulated in terms of potentials:

$$\varepsilon_{out}\frac{\partial\varphi_{out}}{\partial n}-\varepsilon_{in}\frac{\partial\varphi_{in}}{\partial n}=-4\pi\sigma_{ext} \tag{1.14}$$

$$\varphi_{out}=\varphi_{in}\,. \tag{1.15}$$

Equations (1.13), (1.14) and (1.15) describe quasistatic phenomena. As was mentioned above, these equations are true if the terms in the Maxwell equations with spatial derivatives of the field dominate over the terms with temporal derivatives, corresponding to an estimate

$$\lambda\!\!\!^{-}_{0}=\frac{cT}{2\pi}>L\,, \tag{1.16}$$

where c is the speed of light, $\lambda\!\!\!^{-}_{0}$ is the field reduced wavelength in vacuum, T and L are the period of the field oscillations and the characteristic length in the problem, correspondingly. Nanooptic problems deal with structures which are enclosed within lengths $L\sim 50$ nm and fields that change dramatically on this spatial scale. This means that the quasi-static approximation is suitable to describe fields with periods $T>1$ fs or frequencies $\hbar\omega<4$ eV. This covers the whole optical range and below. In other words, the highest frequency in the problem determines the volumes within which the near-field may be described by a quasistatic approximation.

In metals below the plasma frequency - basic nanoplasmonic materials - the magnetic field is enhanced by the larger prefactor in the displacement current (see Eq. (3.4)). This prefactor is inversely proportional to the skin depth

$$l_s\approx\lambda\!\!\!^{-}_{0}\Big/\mathrm{Re}\sqrt{-\varepsilon_m(\omega)}\,, \tag{1.17}$$

where $\varepsilon_m(\omega)$ is the metal dielectric function (for specific definitions of skin depth for different types of waves see Sect. 3.3) [3, 6, 12]. The quasistatic approximation requires the ability to neglect the magnetic term in the Maxwell-Faraday equation (see Eq. (3.2)), which

correspondingly becomes more demanding in plasmonic metals. Inside metal inclusions the relationship (1.16) is supplemented by

$$L_{inc} < l_s . \tag{1.18}$$

This means that the characteristic size L_{inc} of metal inclusions of the structure studied using quasistatic approximation cannot exceed the skin depth. The dependence of the skin depth in silver and gold as a function of frequency at optical frequencies is shown in Figure 1.1.

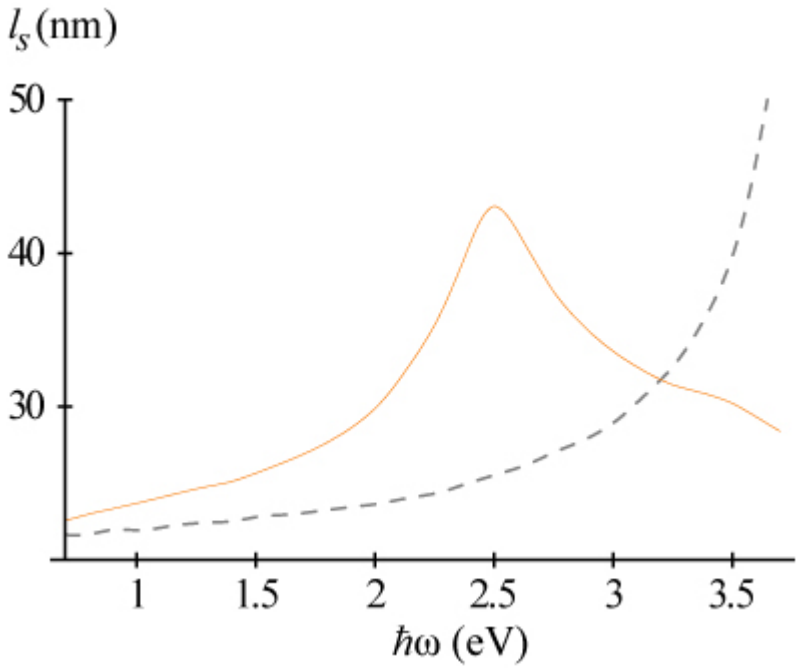

Figure 1.1. (color online) The skin-depth $l_s = \lambda\!\!\!^{-}_0 \big/ \mathrm{Re}\sqrt{-\varepsilon_m}$ in silver (gray broken line) and gold (golden solid line) as a function of frequency. Dielectric permittivities of gold and silver were taken from experimental data [13].

Unfortunately, since the scale on which quasistatics is valid does not extend further than $\lambda\!\!\!^{-}_0$, we are unable to describe the far-zone behavior of the field, leaving scattering and radiation by plasmonic nanostructures out of the scope of quasistatics (see Sect. 3.2). However, quasistatics describes most near-field effects extremely well.

1.2 Spectral Theory of SPs

The general theory based on the quasistatic equation (1.13) in electrically neutral two-component systems ($\rho_{ext} = 0$) originated from attempts to describe the percolation threshold in metal-dielectric composites [14, 15]. It was further developed and used in papers devoted to the studies of Anderson localization of surface plasmons [16], coherent control of optical fields in metal nanostructures [17, 18], surface enhanced Raman scattering (SERS) [19], surface plasmon amplification by stimulated emission of radiation (SPASER) [20, 21]. Following these references, we will describe in this Section the formulas of nanoplasmonic spectral theory required for present work.

Consider a two-component structure consisting of a dielectric host with metal inclusions, whose dielectric function can be written as

$$\varepsilon(\mathbf{r},\omega) = \varepsilon_d + \Theta(\mathbf{r})(\varepsilon_m(\omega) - \varepsilon_d)\,, \tag{1.19}$$

where ε_d and $\varepsilon_m(\omega)$ are bulk dielectric functions of dielectric and metal correspondingly, and $\Theta(\mathbf{r})$ is the function characterizing geometry of the structure, which is equal to 1 if $\mathbf{r}$ is inside the metal, and 0 otherwise.

The structure is surrounded by the surface S (which encloses volume V), so that $\Theta(\mathbf{r})\big|_{\mathbf{r}\in S} = 0$ and $\nabla\Theta(\mathbf{r})\big|_{\mathbf{r}\in S} = 0$. The structure is excited by the external field with potential $\varphi_0(\mathbf{r})$, which satisfies the Laplace equation within the surface S

$$\nabla^2\varphi_0(\mathbf{r}) = 0\,. \tag{1.20}$$

The total potential can be represented as

$$\varphi(\mathbf{r}) = \varphi_0(\mathbf{r}) + \varphi_1(\mathbf{r})\,, \tag{1.21}$$

where $\varphi_1(\mathbf{r})$ is the induced potential, satisfying homogeneous Dirichlet or Neumann conditions at the surface *S*

$$\varphi_1(\mathbf{r})\left(\hat{\mathbf{n}}(\mathbf{r})\cdot\nabla\varphi_1(\mathbf{r})\right)\Big|_{\mathbf{r}\in S}=0, \tag{1.22}$$

where $\hat{\mathbf{n}}(\mathbf{r})$ is a normal ort to surface S at a point $\mathbf{r}$.

With dielectric function (1.19) the operator from Eq. (1.13) becomes

$$\nabla\left(\varepsilon(\mathbf{r},\omega)\nabla\right)=\left(\varepsilon_m(\omega)-\varepsilon_d\right)\left\{\nabla\left(\Theta(\mathbf{r})\nabla\right)-s(\omega)\nabla^2\right\}, \tag{1.23}$$

where $s(\omega)=\left[1-\varepsilon_m(\omega)/\varepsilon_d\right]^{-1}$ is the so-called spectral parameter, which contains all the information about the materials. Substituting potential (1.21) into Eq. (1.13) with $\rho_{ext}=0$ and using Eqs. (1.19) and (1.20) one obtains

$$\nabla\left(\Theta(\mathbf{r})\nabla\varphi_1(\mathbf{r})\right)-s(\omega)\nabla^2\varphi_1(\mathbf{r})=-\nabla\left(\Theta(\mathbf{r})\nabla\varphi_0(\mathbf{r})\right). \tag{1.24}$$

To solve Eq. (1.24) one needs to introduce an eigenproblem

$$\nabla\left(\Theta(\mathbf{r})\nabla\varphi_n(\mathbf{r})\right)-s_n\nabla^2\varphi_n(\mathbf{r})=0, \tag{1.25}$$

where s_n are the eigenvalues, corresponding to eigenfunctions $\varphi_n(\mathbf{r})$, which satisfy boundary condition (1.22). Eigenfunctions, $\varphi_n(\mathbf{r})$, and eigenvalues, s_n, for several geometries are presented in Sect. 2.3.

Multiplying Eq. (1.25) by the complex-conjugate eigenfunction $\varphi_m^*(\mathbf{r})$ and integrating over the volume *V*, we obtain

$$-\int_V\Theta(\mathbf{r})\nabla\varphi_m^*(\mathbf{r})\cdot\nabla\varphi_n(\mathbf{r})dV+s_n\int_V\nabla\varphi_m^*(\mathbf{r})\cdot\nabla\varphi_n(\mathbf{r})dV=0. \tag{1.26}$$

In Eq. (1.26) the surface integrals vanished, since the eigenfunctions satisfy Eq. (1.22) and $\Theta(\mathbf{r})\big|_{\mathbf{r}\in S}=0$. Setting $m=n$ in Eq. (1.26) one obtains an expression for eigenvalues

$$s_n = \frac{\int_V \Theta(\mathbf{r})\left|\nabla \varphi_n(\mathbf{r})\right|^2 dV}{\int_V \left|\nabla \varphi_n(\mathbf{r})\right|^2 dV}. \tag{1.27}$$

Eq. (1.27) shows that the eigenvalue s_n represents the fraction of the eigenmode energy that penetrates the metal constituent of the nanostructure. This implies that s_n are real numbers between 0 to 1.

Equation (1.25) does not contain frequency or any information about materials and it is determined only by the geometry of nanostructure. Eigenfunctions $\varphi_n(\mathbf{r})$ describe fields of the so-called localized surface plasmons (LSP) – electrostatic modes, which have been studied recently in connection with several important nanoscale effects and applications [17, 19-26].

The complex frequencies $\Omega_n = \omega_n - i\gamma_n$ of LSPs can be found as

$$s(\omega_n - i\gamma_n) = s_n. \tag{1.28}$$

If the so-called SP resonance quality factor

$$Q_n = \omega_n / \gamma_n \tag{1.29}$$

is high, $Q_n >> 1$, then one can use a Taylor series to expand $s(\omega_n - i\gamma_n) \approx s(\omega_n) - i\gamma_n \partial s(\omega)/\partial\omega\big|_{\omega=\omega_n} + \ldots$, which gives the following expressions for the resonance frequency ω_n and spectral width γ_n [19, 20, 27]:

$$\mathrm{Re}\, s(\omega_n) = s_n. \tag{1.30}$$

$$\gamma_{st} = \frac{\mathrm{Im}\, s(\omega_n)}{s'(\omega_n)} = \frac{\mathrm{Im}\, \varepsilon_m(\omega)}{\partial\, \mathrm{Re}\, \varepsilon_m(\omega)/\partial\omega}\bigg|_{\omega=\omega_n}, \text{ where } s'(\omega_n) = \frac{\partial\, \mathrm{Re}\, s(\omega)}{\partial\omega}\bigg|_{\omega=\omega_n}. \tag{1.31}$$

Note that, as follows from Eq. (1.31), the SP linewidth (relaxation rate) $\gamma(\omega)$ does not depend on the geometry of the nanostructure and is a function of only frequency. The relaxation

rate $\gamma(\omega)$, related to the SP dephasing time as $\tau(\omega) = 1/(2\gamma(\omega))$, is extremely important in plasmonics and determines the scale of temporal evolution of plasmonic fields, which is $\tau \sim 100\,\text{fs}$ (see also Sect. 5.4). The SP dephasing times determine the ability of SPASER to generate and amplify local fields [20, 21] as well as the local field enhancement $|E/E_0| \propto Q = \omega\tau/2$, where E is the local field and E_0 is the field of the external excitation [28, 29]. This enhancement is especially important for nonlinear processes, for example SERS, whose enhancement factor is $g^R \propto |E/E_0|^4$ [19].

The relaxation time τ may not be determined only by the metal dielectric function [see Eq. (1.31)]. It is additionally influenced by non-local effects for small metal nanoparticles with radii $R \le v_F/\omega \approx 2-5\,\text{nm}$ [8, 9, 11], and by radiative decay for large nanoparticles [29-32]. The quasistatic approximation is invalid for $R \ge l_s \approx 25\,\text{nm}$, but the expression for the relaxation rate (1.31) may be unaffected by radiative decay even for radii larger than l_s, as is shown in Sect. 3.2.

Turning back to spectral theory, let us exchange *m* and *n* and complex-conjugate Eq. (1.26); subtracting the result from Eq. (1.26) we obtain the orthogonality relation between the eigenmodes

$$(s_n - s_m) \cdot \int_V \nabla\varphi_m^*(\mathbf{r}) \cdot \nabla\varphi_n(\mathbf{r}) dV = 0\,. \tag{1.32}$$

It follows from Eq. (1.32) that scalar product of the eigenproblem can be selected as

$$(\phi_1|\phi_2) = \int_V \nabla\phi_2^*(\mathbf{r}) \cdot \nabla\phi_1(\mathbf{r}) dV\,. \tag{1.33}$$

Expression (1.33) satisfies all necessary requirements of the scalar product [19]. The eigenfunctions are orthogonal with respect to the scalar product (1.33) and can be normalized as

$$(\varphi_n|\varphi_m) = \delta_{mn}. \tag{1.34}$$

Consider the retarded Green's function $\overline{G}(\mathbf{r},\mathbf{r}';\omega)$ of the problem given by Eq. (1.24). The Green's function $\overline{G}(\mathbf{r},\mathbf{r}';\omega)$ should satisfy the following equation

$$\left(\nabla\Theta(\mathbf{r})\nabla - s(\omega)\nabla^2\right)\overline{G}(\mathbf{r},\mathbf{r}';\omega) = \delta(\mathbf{r}-\mathbf{r}'), \tag{1.35}$$

as well as the boundary conditions (1.22). It can be expanded over the eigenfunctions $\varphi_n(\mathbf{r})$ in the form

$$\overline{G}(\mathbf{r},\mathbf{r}';\omega) = \sum_n a_n(\mathbf{r}';\omega)\varphi_n(\mathbf{r}). \tag{1.36}$$

Substituting expression (1.36) into Eq. (1.35), multiplying by $\varphi_m^*(\mathbf{r})$ and integrating over *V*, we obtain $a_m(\mathbf{r}';\omega)(s(\omega)-s_m) = \varphi_m^*(\mathbf{r}')$ and, correspondingly, for the Green's function [19]

$$\overline{G}(\mathbf{r},\mathbf{r}';\omega) = \sum_n \frac{\varphi_n(\mathbf{r})\varphi_n^*(\mathbf{r}')}{s(\omega)-s_n}. \tag{1.37}$$

Two features of expansion (1.37) are important [19]. First, it separates the dependencies on geometry and material properties. The geometrical properties of the nanosystem enter only through the eigenfunctions $\varphi_n(\mathbf{r})$ and eigenvalues s_n which are independent of the material properties. Therefore they can be computed for a given geometry only once, which simplifies and accelerates further computations. Complementarily, the material properties of the system are present in Eq. (1.37) only through a single function: the spectral parameter $s(\omega)$. The second important feature of Eq. (1.37) is that this Green's function satisfies exact analytical properties due to the form of Eq. (1.37) that contains only simple poles in the lower half-plane of the complex frequency ω and does not have any singularities in the upper half-plane of ω. Consequently, G is a retarded Green's function that automatically guarantees the causality of

the results of time-dependent calculations. Namely, the Green's function in the time domain satisfies the condition $\overline{G}(\mathbf{r},\mathbf{r}';t)=0$ for $t<0$.

The induced potential $\varphi_1(\mathbf{r})$ in the nanostructure can be expressed through Green's function (1.37) [19]

$$\varphi_1(\mathbf{r})=-\int_V \overline{G}(\mathbf{r},\mathbf{r}';\omega)\frac{\partial}{\partial \mathbf{r}'}\left(\Theta(\mathbf{r}')\frac{\partial\varphi_0(\mathbf{r}')}{\partial\mathbf{r}'}\right)d^3r', \tag{1.38}$$

where $\partial/\partial\mathbf{r}\equiv\nabla$. Correspondingly, the total potential (1.21) assumes the form

$$\varphi(\mathbf{r})=\varphi_0(\mathbf{r})-\int_V \overline{G}(\mathbf{r},\mathbf{r}';\omega)\frac{\partial}{\partial \mathbf{r}'}\left(\Theta(\mathbf{r}')\frac{\partial\varphi_0(\mathbf{r}')}{\partial\mathbf{r}'}\right)d^3r', \tag{1.39}$$

Integrating this relation by parts twice and using $\Theta(\mathbf{r})\big|_{\mathbf{r}\in S}=0$ we get

$$\varphi(\mathbf{r})=\varphi_0(\mathbf{r})-\int_V \varphi_0(\mathbf{r}')\frac{\partial}{\partial \mathbf{r}'}\left(\Theta(\mathbf{r}')\frac{\partial}{\partial\mathbf{r}'}\overline{G}(\mathbf{r},\mathbf{r}';\omega)\right)d^3r', \tag{1.40}$$

Relation (1.12) allows one to obtain the closed expression for the total optical field $\mathbf{E}(\mathbf{r})$ in terms of the excitation field $\mathbf{E}_0(\mathbf{r})$

$$E_\alpha(\mathbf{r})=E_{0\alpha}(\mathbf{r})+\int_V \overline{G}_{\alpha\beta}(\mathbf{r},\mathbf{r}';\omega)\Theta(\mathbf{r}')E_{0\beta}(\mathbf{r}')d^3r', \tag{1.41}$$

where the dyadic Green's function is [19]

$$\overline{G}_{\alpha\beta}(\mathbf{r},\mathbf{r}';\omega)=\frac{\partial^2}{\partial r_\alpha\partial r'_\beta}\overline{G}(\mathbf{r},\mathbf{r}';\omega), \tag{1.42}$$

Now let us substitute the expansion (1.37) into Eq. (1.40)

$$\varphi(\mathbf{r})=\varphi_0(\mathbf{r})-\sum_n\frac{\varphi_n(\mathbf{r})}{s(\omega)-s_n}\cdot\int_V \varphi_0(\mathbf{r}')\frac{\partial}{\partial \mathbf{r}'}\left(\Theta(\mathbf{r}')\frac{\partial\varphi_n^*(\mathbf{r}')}{\partial\mathbf{r}'}\right)d^3r', \tag{1.43}$$

and using eigenproblem (1.25) we obtain [19]

$$\varphi(\mathbf{r}) = \varphi_0(\mathbf{r}) - \sum_n \frac{s_n}{s(\omega) - s_n} \varphi_n(\mathbf{r}) \cdot \int_V \varphi_0(\mathbf{r}') \frac{\partial^2 \varphi_n^*(\mathbf{r}')}{\partial^2 \mathbf{r}'} d^3 r', \tag{1.44}$$

This expression can be rewritten in the form

$$\varphi(\mathbf{r}) = \varphi_0(\mathbf{r}) - \int_V \varphi_0(\mathbf{r}') \frac{\partial^2}{\partial^2 \mathbf{r}'} G(\mathbf{r}, \mathbf{r}'; \omega) d^3 r', \tag{1.45}$$

where $G(\mathbf{r}, \mathbf{r}'; \omega)$ is another retarded Green's function [19]

$$G(\mathbf{r}, \mathbf{r}'; \omega) = \sum_n \frac{s_n}{s(\omega) - s_n} \varphi_n(\mathbf{r}) \varphi_n^*(\mathbf{r}'). \tag{1.46}$$

It is shown in the next Chapter [see Eq. (2.7)] that the Green's function (1.46) determines the renormalization of a quasistatic interaction in the vicinity of metal nanostructures.

Chapter 2. Nanoplasmonic Enhancement of Coulomb Interaction

2.1 Quasistatic Interaction on the Nanoscale

Nanostructured plasmonic metal systems are known to enhance greatly a variety of radiative and non-radiative optical processes, both linear and nonlinear, which are due to the interaction of an electron in a molecule or semiconductor with the enhanced local optical field of the surface plasmons (SPs). Among them are surface-enhanced Raman scattering (SERS) [19, 33-37], SP-enhanced fluorescence [38-42], fluorescence quenching in the proximity of metal surfaces [38, 41, 43], coherent anti-Stokes Raman scattering (CARS) [44], surface-enhanced hyper-Raman scattering (SEHRS) [45], etc. These are distinctly different from numerous many-body phenomena that are due to the Coulomb interaction between charged particles: carriers (electrons and holes) and ions. These include carrier–carrier or carrier–ion scattering, energy and momentum transfer (including the drag effect), thermal equilibration, exciton formation, impact ionization and Auger effects [15].

It is not widely recognized that these and other many-body effects can also be modified and enhanced by the SP local fields. A special but extremely important class of such many-body phenomena is constituted by chemical reactions at metal surfaces, including catalytic reactions. In the paper [46] we have proposed a general and powerful theory of the plasmonic enhancement of the many-body phenomena resulting in a closed expression for the SP-dressed Coulomb interaction. Metal-dielectric nanoshells are extremely important for modern nanotechnology [47]. We illustrate our theory by computing the dressed interaction explicitly for metal-dielectric

nanoshells, which exhibits a rich resonant behavior in both the magnitude and phase. This interaction is used to describe the nanoplasmonic-enhanced Förster resonant energy transfer (FRET) between nanocrystal quantum dots (NQDs) in proximity to a plasmonic nanoshell. This is of great interest for plasmonic-enhanced solar cells and light-emitting devices [48]. Catalysis at nanostructured metal surfaces, nonlocal carrier scattering, and SERS are discussed in this thesis among other effects and applications where the nanoplasmonic renormalization of the Coulomb interaction may be of principal importance.

2.2 Plasmonic Renormalization of Coulomb Interaction

Consider a system of charged particles situated in the vicinity of a plasmonic metal nanosystem. For definiteness, we will assume that these particles are electrons, although they can also be holes or ions of the lattice. One of the examples of such systems is a semiconductor in proximity to a nanostructured metal surface. When an electron undergoes a transition with some frequency ω, this transition is accompanied by local electric fields oscillating with the same frequency. These fields excite SP modes with the corresponding frequencies whose fields overlap in space with the transition fields. A property of these SP eigenmodes is that they can be delocalized over the entire nanostructure [16]. The local optical fields of the SPs can excite a resonant transition of another electron. This process, which in the quantum mechanical language is the electron–electron interaction by the exchange of an SP quantum, renormalizes ('dresses') the direct interaction between these two charges. As a result, the direct ('bare') Coulomb interaction between the electrons, $V(\mathbf{r}-\mathbf{r}') = 1/\left(\varepsilon_d |\mathbf{r}-\mathbf{r}'|\right)$, where ε_d is the dielectric constant of the embedding medium, is replaced by the dressed interaction $W(\mathbf{r},\mathbf{r}';\omega)$. This dressed interaction is generally not translationally invariant, i.e., it depends on the coordinates $\mathbf{r}$ and $\mathbf{r}'$

of both electrons; it also depends on the transition frequency ω. Note that W is generally a complex function, and its phase describes a delay inherent in the plasmonic reaction. This phase varies sharply across plasmonic resonances, as we will show later in this paper.

We schematically illustrate this SP-mediated electron–electron interaction in Figure 2.1, where we show electrons in two semiconductor NQDs situated at the surface of a metal nanostructure. The plasmonic fields, indicated by orange, excited by one of the electrons interact with the other one in a different NQD. The interacting charges could also belong to the same quantum dot and could be not only electrons but also holes.

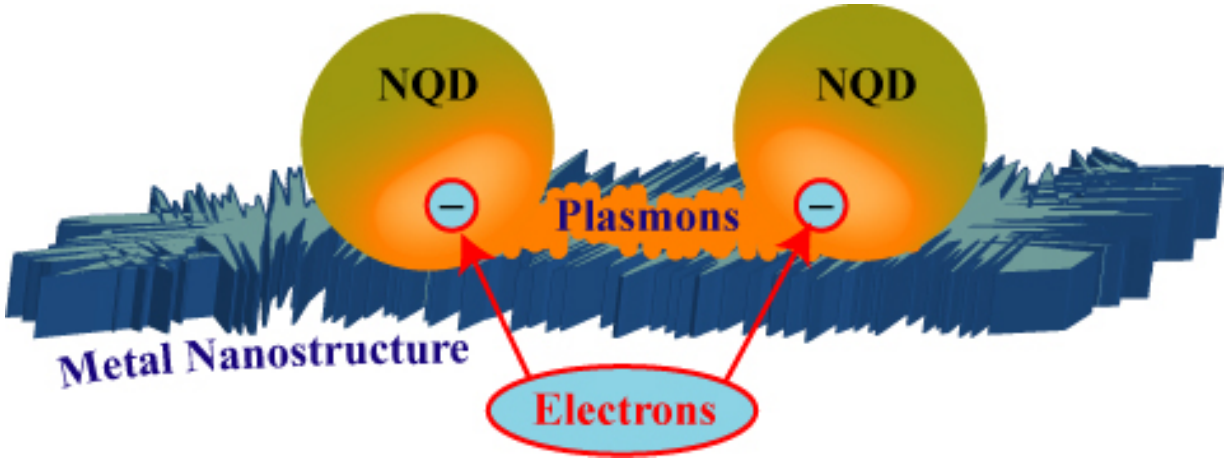

Figure 2.1. (color online) Schematic of metal nanostructure and semiconductor nanocrystal quantum dots (NQDs) situated in its vicinity. The metal nanostructure is depicted by the dark blue color. Two electrons are indicated in NQDs by the blue color and the local plasmonic fields are schematically shown by the orange color.

The resonant nature of the electron-plasmon interaction may lead to the significant enhancement of the dressed interaction W with respect to the bare one, V. A typical SP eigenmode tends to form 'hot spots' of the local fields separated by distances on the order of the size of the entire plasmonic nanostructure [16]. Therefore one should expect that the dressed interaction will also be delocalized over such distances, i.e., be relatively much more long-ranged than the bare Coulomb interaction.

The dressed interaction $W(\mathbf{r},\mathbf{r}';\omega)$, by definition, is the potential created at a point $\mathbf{r}$ by a charge positioned at another point $\mathbf{r}'$ and oscillating with frequency ω. We assume that the size of the system is much smaller than any relevant electromagnetic length (radiation wavelength, skin depth, etc) and will use the quasistatic approximation, which is conventional in nanoplasmonics. In this case, *W* satisfies the continuity equation

$$\frac{\partial}{\partial \mathbf{r}}\left[\varepsilon(\mathbf{r},\omega)\frac{\partial}{\partial \mathbf{r}}W(\mathbf{r},\mathbf{r}';\omega)\right]=-4\pi\delta(\mathbf{r}-\mathbf{r}'), \tag{2.1}$$

where the dielectric function $\varepsilon(\mathbf{r},\omega)$ is given by Eq. (1.19).

Now let us represent the *W* as a sum of the 'bare' Coulomb potential *V* and the additional interaction *R* due to the nanostructure

$$W(\mathbf{r},\mathbf{r}';\omega)=V(\mathbf{r}-\mathbf{r}')+R(\mathbf{r},\mathbf{r}';\omega). \tag{2.2}$$

With dielectric permittivity in the explicit form (1.19) Eq. (2.1) reads

$$\frac{\partial^2}{\partial^2 \mathbf{r}}W(\mathbf{r},\mathbf{r}';\omega)-\frac{1}{s(\omega)}\frac{\partial}{\partial \mathbf{r}}\left[\Theta(\mathbf{r})\frac{\partial}{\partial \mathbf{r}}W(\mathbf{r},\mathbf{r}';\omega)\right]=-\frac{4\pi}{\varepsilon_d}\delta(\mathbf{r}-\mathbf{r}'). \tag{2.3}$$

Using Eq. (2.3) and the fact that

$$\frac{\partial^2}{\partial^2 \mathbf{r}}V(\mathbf{r}-\mathbf{r}')=-\frac{4\pi}{\varepsilon_d}\delta(\mathbf{r}-\mathbf{r}'), \tag{2.4}$$

we obtain

$$\frac{\partial}{\partial \mathbf{r}}\left[\Theta(\mathbf{r})\frac{\partial}{\partial \mathbf{r}}R(\mathbf{r},\mathbf{r}';\omega)\right]-s(\omega)\frac{\partial^2}{\partial^2 \mathbf{r}}R(\mathbf{r},\mathbf{r}';\omega)=-\frac{\partial}{\partial \mathbf{r}}\left[\Theta(\mathbf{r})\frac{\partial}{\partial \mathbf{r}}V(\mathbf{r}-\mathbf{r}')\right]. \tag{2.5}$$

Eq. (2.5) is similar to Eq. (1.24). Therefore, *W* can be written by analogy with Eq. (1.45)

$$W(\mathbf{r},\mathbf{r}';\omega)=V(\mathbf{r}-\mathbf{r}')-\int_V V(\mathbf{r}''-\mathbf{r}')\frac{\partial^2}{\partial^2 \mathbf{r}''}G(\mathbf{r},\mathbf{r}'';\omega)d^3r'', \tag{2.6}$$

where $G(\mathbf{r},\mathbf{r}';\omega)$ is the Green's function given by (1.46).

If the system is in an infinite space (or the boundaries are remote enough), then the use of Green's identity in Eq. (2.6) simplifies it to the form [46]

$$W(\mathbf{r},\mathbf{r}';\omega)=V(\mathbf{r}-\mathbf{r}')+\frac{4\pi}{\varepsilon_d}G(\mathbf{r},\mathbf{r}';\omega)= \\ =\frac{1}{|\mathbf{r}-\mathbf{r}'|}+\frac{4\pi}{\varepsilon_d}\sum_n\frac{s_n}{s(\omega)-s_n}\varphi_n(\mathbf{r})\varphi_n^*(\mathbf{r}'). \tag{2.7}$$

This is a simple, yet general and powerful result: the Coulomb interaction is renormalized by the full retarded Green's function (1.46) whose contraction also describes the nanoplasmonic enhancement of SERS and other optical phenomena. The poles of the Green's function (1.46) correspond to the SP modes whose frequencies ω_n are given by the equation $s(\omega_n)=s_n$. Close to such frequencies, G becomes large, proportional to the quality factor Q_n of the SP resonance [19]. This describes the plasmonic renormalization and enhancement of the dressed Coulomb interaction.

2.3 Examples of Nanoplasmonic Renormalization

We will illustrate the plasmonic renormalization and enhancement of the Coulomb interaction near several nanoplasmonic systems. Let us start with metal nanoshell. Such nanoshells have significant fundamental and applied interest [47]. Eigenfunctions for nanoshells are products of the radial power functions and spherical harmonics that describe the angular dependence $\varphi_{lm}^{\pm}=R_l^{\pm}(r)Y_{lm}(\hat{\mathbf{r}})$. We express the radial functions in the following form

$$R_l^{\pm}(r)=\sqrt{\frac{f_l^{\pm}}{(2l+1)a}}\begin{cases} A_l^{\pm}(r/a)^l, & \text{if } r<b \\ \left(B_l^{\pm}(r/a)^l+C_l^{\pm}(a/r)^{l+1}\right), & \text{if } b<r<a, \\ (a/r)^{l+1}, & \text{if } r>a \end{cases} \tag{2.8}$$

where b is the inner and a is the outer radius of the nanoshell, and $f_l^{\pm}$ are normalization factors.

According to (1.25) the eigenvalues $s_l^{\pm}$ and coefficients $A_l^{\pm}$, $B_l^{\pm}$, $C_l^{\pm}$ in (2.8) can be found by solving the system of boundary equations (1.14) and (1.15)

$$s_l^{\pm} = \frac{l + (1 \mp \lambda)/2}{2l+1},\ A_l^{\pm} = \frac{2(l+1)(\pm\lambda - 1)}{\lambda^2 - 1},\ B_l^{\pm} = \frac{2(l+1)}{2l+1 \pm \lambda}, \tag{2.9}$$

$$C_l^{\pm} = \frac{(\lambda^2 - 1)}{\lambda^2 - 1 + 2(l+1)(1 \pm \lambda)}, \text{ where } \lambda = \sqrt{1 + 4l(l+1)(b/a)^{2l+1}}\ .$$

The $P = \pm$ in the notations corresponds to classification of the modes with respect to their radial behavior: the "plus" modes oscillate in phase at different surfaces of the nanoshell, while "minus" modes are out of phase at different boundaries. Indeed, consider the case of extremely thin nanoshell, so that $b/a \to 1$:

$$\lambda \to 2l+1,\ s_l^{\pm} \to (1 \mp 1)/2,\ A_l^{\pm} \to \pm 1 - (1 \mp 1)/(2l), \tag{2.10}$$

$$B_l^{\pm} \to \frac{2(l+1)}{(2l+1)(1 \pm 1)},\ C_l^{\pm} \to \frac{2l}{(2l+1)(1 \pm 1)}.$$

Formulas (2.10) clearly confirm the statement given in the previous paragraph about the radial behavior of eigenfunctions. Note that according to discussion after Eq. (1.27) the "plus" mode is absolutely outside of the shell, since $s_l^{+} \to 0$, while the "minus" mode is entirely squeezed into the thin nanoshell.

The eigenfunctions should be normalized by condition (1.34). It can be accomplished using the identities [3]

$$\int_0^{\pi} P_{l'}^m \cdot P_l^m \cdot \sin\theta \cdot d\theta = \frac{2}{2l+1} \cdot \frac{(l+m)!}{(l-m)!} \cdot \delta_{l'l}\ . \tag{2.11}$$

$$\int_0^{\pi} \left(\frac{\partial P_{l'}^m}{\partial \theta} \cdot \frac{\partial P_l^m}{\partial \theta} + \frac{m^2 \cdot P_{l'}^m \cdot P_l^m}{\sin^2 \theta} \right) \cdot \sin\theta \cdot d\theta = \frac{2}{2l+1} \cdot \frac{(l+m)!}{(l-m)!} \cdot l(l+1) \cdot \delta_{l'l}\ . \tag{2.12}$$

This leads to the following normalization condition for radial functions

$$\int \nabla \varphi^{P}_{l'm'} \cdot \nabla \varphi^{P}_{lm} \cdot d\Omega = \left\{ \left(\frac{\partial R^{P}_{l}}{\partial r} \right)^2 + \frac{l(l+1)}{r^2} \cdot R^{P\,2}_{l} \right\} \cdot \delta_{l'l} \delta_{m'm} = \delta_{PP'} \delta_{l'l} \delta_{m'm} . \tag{2.13}$$

From (2.13) we have calculated the normalization factors in (2.8):

$$f^{\pm}_{l} = \pm \frac{(\pm\lambda + 1)(2l + 1 \pm \lambda)}{4\lambda(l+1)} . \tag{2.14}$$

Now let us study a very significant example of a nanosphere. In this case only the $P = +$ mode represents physically sensible solution, whose eigenvalues for nanosphere are $s_l = l/(2l+1)$. The radial function is in this case

$$R_l = (2l+1)^{-1/2} a^{-1/2} \begin{cases} (r/a)^l, \text{if } r < b \\ (a/r)^{l+1} \text{ if } r > a \end{cases} . \tag{2.15}$$

Therefore, the renormalized Coulomb interaction (2.7) near the metal nanosphere is

$$W(\mathbf{r}, \mathbf{r}'; \omega) = V(\mathbf{r} - \mathbf{r}') + \frac{4\pi}{\varepsilon_d a} \sum_{lm} \frac{l/(2l+1)^2}{s(\omega) - l/(2l+1)} \begin{pmatrix} (a/r)(r'/r)^l \\ (a^2/rr')^{l+1} \end{pmatrix} \cdot Y_{lm}(\mathbf{r}) Y^{*}_{lm}(\mathbf{r}') , \tag{2.16}$$

where $r > a$ is the radius of the source and r' is the potential observation point. The upper value is for $r' < a$, and the lower for $r' > a$. At $\omega \to 0$ the metal dielectric function diverges, therefore $s(0) \to 0$. This simplifies Eq. (2.16) at $r' > a$ to

$$W(\mathbf{r}, \mathbf{r}'; \omega) = V(\mathbf{r} - \mathbf{r}') - \frac{4\pi}{\varepsilon_d a} \sum_{lm} \frac{1}{(2l+1)} \left(\frac{a^2}{rr'} \right)^{l+1} \cdot Y_{lm}(\mathbf{r}) Y^{*}_{lm}(\mathbf{r}') = \tag{2.17}$$

$$= \frac{1}{\varepsilon_d |\mathbf{r} - \mathbf{r}'|} - \frac{(a/r')}{\varepsilon_d \cdot |\mathbf{r} - (a^2/r'^2)\mathbf{r}'|} ,$$

The last part of Eq. (2.17) is the Green's function of the Poisson equation for a Dirichlet problem which can be also obtained through the method of mirror charges [2, 6].

In general, formula (2.7) in the limit $s(\omega) \to 0$ gives the expression for static interaction in the vicinity of a perfect conductor

$$W(\mathbf{r},\mathbf{r}';\omega)=\frac{1}{\varepsilon_d|\mathbf{r}-\mathbf{r}'|}-\frac{4\pi}{\varepsilon_d}\sum_n\varphi_n(\mathbf{r})\varphi_n^*(\mathbf{r}')\,. \tag{2.18}$$

Another interesting situation occurs when considering a thin metal film embedded into a dielectric. The eigenfunctions in cylindrical coordinates have the form $\varphi_{km}^{\pm}=g_k^{\pm}(z)J_m(k\rho)e^{im\phi}$, where axis z is orthogonal to the film and the film is in the $|z|\le d/2$ region. If the dielectric on both sides of the film is the same, the eigenstates are even or odd with respect to transformation $z\to -z$ and denoted with "+" or "-", correspondingly. The behavior of eigenstates in perpendicular to the film direction is described by

$$g_k^{\pm}=\sqrt{f_k^{\pm}}\begin{cases}\pm e^{k(z+d/2)}, \text{ if } z<-d/2\\ \mathrm{tr}_{\pm}(kz)/\mathrm{tr}_{\pm}(kd/2), \text{ if } z<|d/2|\text{, where } \mathrm{tr}_+=\cosh,\ \mathrm{tr}_-=\sinh\\ e^{-k(z-d/2)} \text{ if } z>d/2\end{cases} \tag{2.19}$$

Boundary conditions (1.14)-(1.15) give the following eigenvalues

$$s_k^{\pm}=\frac{1}{2}(1\mp e^{-kd})\,. \tag{2.20}$$

Normalization of eigenfunctions $\varphi_{km}^{\pm}$ can be achieved using the formula

$$\int\varphi_{km}^{P}(\varphi_{k'm'}^{P'})^*\rho d\rho d\phi dz=f_k^{\pm}\cdot 2k\left(1+\frac{\mathrm{tr}_{\mp}(kd/2)}{\mathrm{tr}_{\pm}(kd/2)}\right)\delta_{PP'}\cdot 2\pi\delta_{mm'}\frac{1}{k}\delta(k-k')= \tag{2.21}$$
$$=\delta_{PP'}\delta_{mm'}\delta(k-k'),$$

so that

$$f_k^{+}=\frac{1}{4\pi(1+\tanh(kd/2))}\ \text{ and }\ f_k^{-}=\frac{1}{4\pi(1+\coth(kd/2))}\,. \tag{2.22}$$

Now let us consider a point source at $z=d/2+h>d/2$ and see what is the potential at the other side of the film at the frequency of plasmon resonance of a flat surface, i.e. when $\varepsilon_m(\omega_{sp})=-\varepsilon_d$ or $s(\omega_{sp})=1/2$.

$$W(z=h+d/2, z'<-d/2; \omega=\omega_{sp}) = \frac{1}{\varepsilon_d \sqrt{\rho'^2 + (z'-h-d/2)^2}} + \tag{2.23}$$

$$+\frac{4\pi}{\varepsilon_d}\int_0^\infty dk\,\frac{J_0(k\rho')}{4\pi} e^{-kh}\left(\frac{(1+e^{-kd})}{e^{-kd}}\frac{e^{k(z'+d/2)}}{(1+\coth(kd/2))} + \frac{(1-e^{-kd})}{e^{-kd}}\frac{e^{k(z'+d/2)}}{(1+\tanh(kd/2))}\right) =$$

$$= \frac{1}{\varepsilon_d \sqrt{\rho'^2 + (z'-h-d/2)^2}} + \frac{4\pi}{\varepsilon_d}\int_0^\infty dk\,\frac{J_0(k\rho')}{4\pi} e^{-k(h-z')} e^{-kd/2}(-1+e^{2kd}).$$

Using the relation $1/\sqrt{\rho^2+z^2} = \int_0^\infty dk \cdot e^{-kz} J_0(k\rho)$ [49], we arrive at

$$W(z=h+d/2, z'<h-3d/2; \omega=\omega_{sp}) = \frac{1}{\varepsilon_d \sqrt{\rho'^2 + (h-3d/2-z')^2}}. \tag{2.24}$$

Formula (2.24) implies, that an ideal three-dimensional image of the source charge is formed behind the film at distance $d-h$ from the film [8]. This shows that the theory of the renormalized Coulomb interaction can be used for further studies of imaging by metal nanostructures.

Let us turn back to metal nanoshell. Using (2.8) and (2.9) we have obtained [46] the renormalized Coulomb potential $W(\mathbf{r},\mathbf{r}';\omega)$ for $r, r' > a$, where a is the external radius of the nanoshell, to be [46]

$$W(\mathbf{r},\mathbf{r}';\omega) = V(\mathbf{r}-\mathbf{r}') + \frac{4\pi}{\varepsilon_d a}\sum_{lm}\frac{F_l(x,\omega)}{2l+1}\left(\frac{a^2}{rr'}\right)^{l+1} Y_{lm}(\mathbf{r})Y_{lm}^*(\mathbf{r}'). \tag{2.25}$$

Analogous expressions for the r and/or r' belonging to the inner part of the shell also have been obtained and used in the computations, in particular, those illustrated in Figure 2.3. In (2.25), the spherical harmonics Y_{lm} depend only on the directions of the corresponding vectors, and x is the shell aspect ratio (i.e. the ratio of the inner to outer shell radius). The form factor F_l is given by an exact resonant pole expression:

$$F_l(x,\omega) = \frac{s_l^+ f_l^+}{s(\omega) - s_l^+} + \frac{s_l^- f_l^-}{s(\omega) - s_l^-}, \tag{2.26}$$

where $P = \pm$ refers to the symmetry of the corresponding SP mode, eigenvalues $s_l^{\pm}$ are given in (2.9) and normalization factors $f_l^{\pm}$ are given by Eq. (2.14).

Note that SP eigenmodes with the $P = +$ symmetry have dominating oscillator strength in the long-wavelength (red and near-IR) part of the spectrum, where the quality factors of the SP resonances for noble metals are high, and which are most important in many cases.

We demonstrate the renormalization of the Coulomb interaction near thin metal-dielectric nanoshell with radius $a = 20\,\text{nm}$ and aspect ratio $x = 0.9$ in Figure 2.2. Two charges in a dielectric matrix with $\varepsilon_d = 2$ are separated by the distance $6\,\text{nm}$ and placed at positions with radii $r = r' = 22\,\text{nm}$. The renormalized interaction (orange curve in Figure 2.2(a)) is several times larger in magnitude than the bare Coulomb interaction $V = 1/12\ \text{nm}^{-1}$ (light violet curve in Figure 2.2(a)) and is extremely large at the dipole SP resonance, with $|W| \approx 1\ \text{nm}^{-1}$. Note the change of phase of the interaction at the SP resonances, where screening is substituted by anti-screening.

We depict the resonant behavior and renormalization (enhancement) of the Coulomb interaction in Figure 2.3 for a silver nanoshell with aspect ratio $x = 0.9$ deposited on a dielectric core with permittivity $\varepsilon_d = 2$ embedded into a host with the same permittivity. The silver dielectric function is adopted from the experimental data [13]. For this specific nanoshell, the lowest dipole eigenmode (quantum numbers $L = 1$, $P = -$) has eigenfrequency $\hbar\omega_{1-} = 1.60$ eV. For a red-detuned (from the dipole SP resonance) electronic transition frequency $\hbar\omega = 1.5$ eV, the renormalized interaction is displayed in Figure 2.3 (a). Very close to the singular point $\mathbf{r} = \mathbf{r}'$,

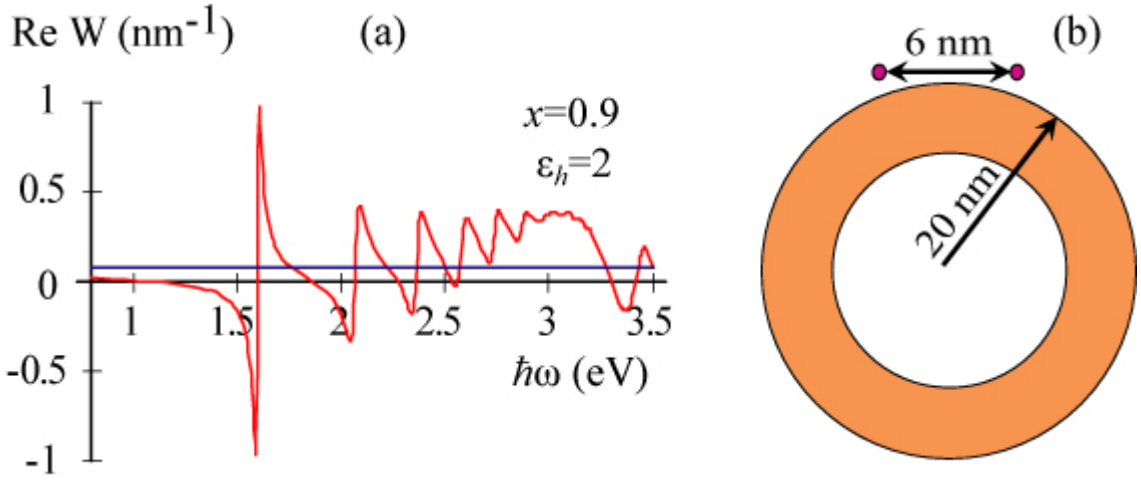

Figure 2.2. (color online) Renormalization of Coulomb interaction between two charges in a dielectric matrix with $\varepsilon_d = 2$ positioned at coordinates $\{x, y\} = \{\pm 3\,\mathrm{nm}, 22\,\mathrm{nm}\}$ near a metal-dielectric nanoshell. (a) The bare Coulomb interaction $V = 1/12\,\mathrm{nm}^{-1}$ (light violet) and renormalized interaction (orange). The renormalized interaction is an order of magnitude larger than the Coulomb interaction near the dipole plasmonic resonance. (b) Schematic of the nanostructure.

the renormalization is reduced to conventional dielectric screening: this is displayed by the opposite sign (blue color in the panel) of $\mathrm{Re}W(\mathbf{r},\mathbf{r}';\omega)$ with respect to the bare Coulomb potential (the red dot pointed to by the arrow). On the opposite side of the nanosphere, there is a 'mirror image' of the dressed interaction potential ReW oscillating in phase (as indicated by the red color) with the initial field. This shows that the nanoplasmonic effects greatly extend the range of the dressed Coulomb interaction. This is due to the delocalization the dipole eigenmode, which defines the nanoplasmonic effects in this spectral region.

For $\hbar\omega = 1.59$ eV, which is very close to (but still red-detuned from) the dipole SP resonance, the real part of the renormalized Coulomb interaction potential, $\mathrm{Re}W(\mathbf{r},\mathbf{r}';\omega)$ is displayed in Figure 2.3(b). In this case, the dynamic screening of the bare potential becomes very strong, which is seen from the diminished magnitude and radius of the Coulomb potential shown

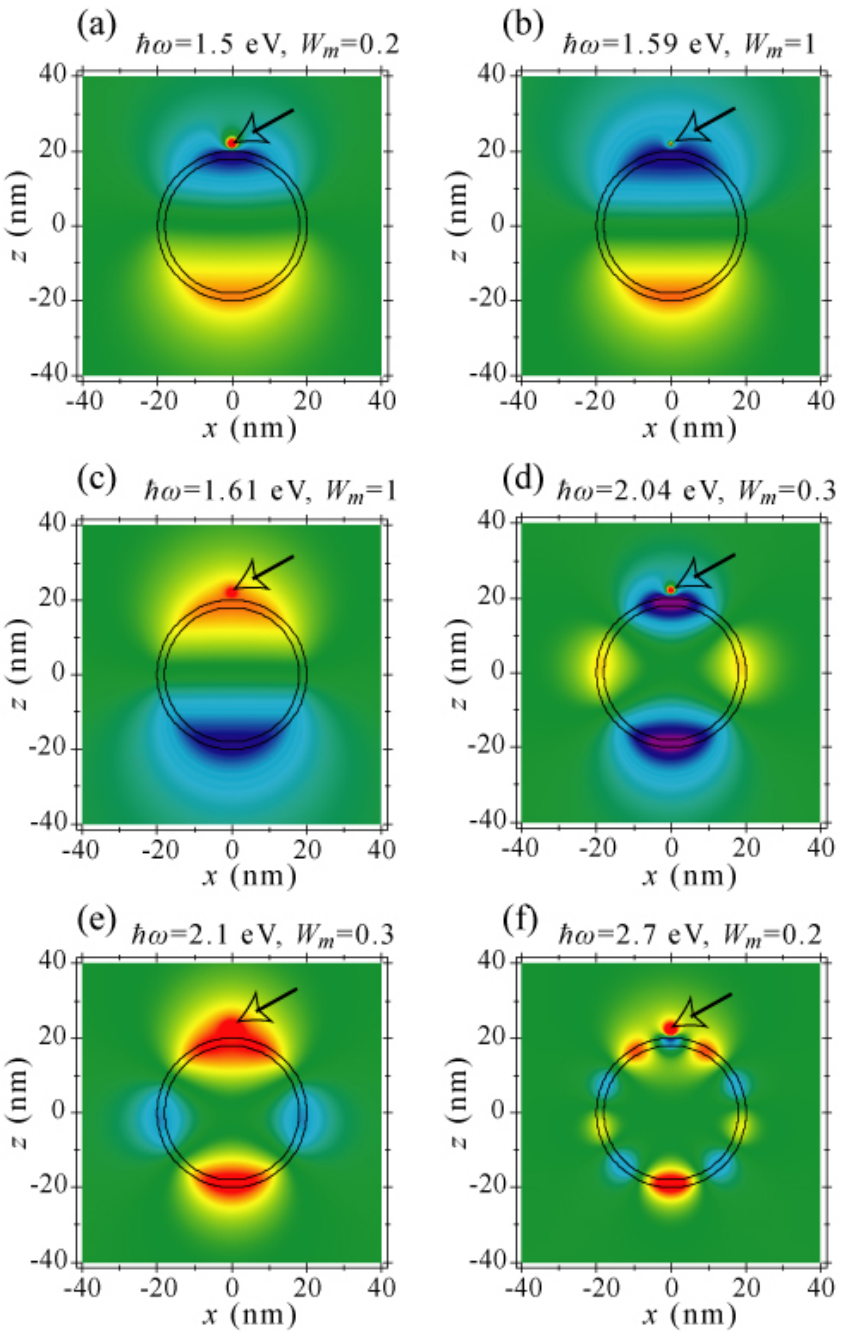

Figure 2.3. (color online) Renormalized (dressed) Coulomb interaction $\mathrm{Re}W(\mathbf{r},\mathbf{r}';\omega)$ for a silver nanoshell of aspect ratio $x=0.9$. Point $\mathbf{r}'$ is fixed and indicated by the black arrows in the upper parts of the panels. The dependence of $\mathrm{Re}W(\mathbf{r},\mathbf{r}')$ on $\mathbf{r}=\{x,z\}$ is shown by color coding in the panels for the cross section of the shell. The limits of this color coding are $\pm W_m$; the maximum W_m and higher values of $\mathrm{Re}W$ are depicted by red, and the minimum $-W_m$ and lower values of $\mathrm{Re}W$ are shown by blue. Frequencies ω are indicated in the panels.

as the small red dot indicated by the arrow. The *W* interaction, however, is strongly delocalized both around the point $\mathbf{r}'$, where the charge is situated (manifested by the intense blue 'cloud') and at the opposite pole of the nanoshell, where the sign of the interaction is the same as that for the bare charge (red color).

As frequency ω increases further (Figure 2.3(d)–(f)), higher multipole SP eigenmodes start to contribute to the Coulomb potential dressing, starting with the quadrupole in panels (d) and (e). In all the cases, the screening in the vicinity of the charge for frequencies to the red of the resonance changes to the anti-screening for the blue spectral detuning. The dressed potential is delocalized over the surface of the nanoshell, thus becoming extremely long-ranged. This is a general property of the nanoplasmonic renormalization of the Coulomb interaction: the range of the dressed interaction always extends over the entire nanoplasmonic system. This effect is due to the absence of the strong localization of the SP eigenmodes [16].

In Figure 2.3, we have plotted only the real part of the renormalized Coulomb potential $W(\mathbf{r},\mathbf{r}';\omega)$. However, its imaginary part (not shown) is also important. In the resonant cases, it is greatly enhanced and delocalized over the entire nanosystem. Because of the underlying $\pi/2$ phase shift, it does not interfere with the real part of *W*. It always increases the strength and contributes to the delocalization of the dressed interaction.

2.4 Giant Förster Energy Transfer near Metal-Dielectric Nanoshells

One of the many-body effects that is affected by the nanoplasmonic renormalization of the Coulomb interaction is the FRET [50, 51]. It has been proposed theoretically [52, 53] and observed experimentally [38] that the Förster transfer between chromophores in the proximity of a metal spheroid is enhanced by the SP effect. Note that SP-mediated energy transfer across a

metal film has also been observed [54]. Below, as an illustration of our general theory [46], we consider FRET for chromophores at the surface of a metal/dielectric nanoshell. As we have already mentioned, the nanoshells are spectrally tunable and can have their SP eigenmodes shifted in frequency to the red and near-IR spectral regions [47], which results in increased values of the resonance quality factor due to lower dielectric losses in the metal [13], and, hence, enhanced plasmonic effects.

The FRET is an electron–electron interaction (many-body) effect that is due to dipole electronic transitions. It is described by a Hamiltonian that is a dipolar expansion of the interaction equation (2.7) [1]:

$$H'_{FRET} = \left(\mathbf{d}_d \frac{\partial}{\partial \mathbf{r}} \right) \left(\mathbf{d}_a \frac{\partial}{\partial \mathbf{r}'} \right) W(\mathbf{r}, \mathbf{r}'; \omega), \tag{2.27}$$

where $\mathbf{d}_d$ and $\mathbf{d}_a$ are the dipole operators of the two interacting electrons (the energy donor and acceptor) at points $\mathbf{r}$ and $\mathbf{r}'$, respectively. Note that the SPs of all multipolarities are taken into account by equation (2.27).

For specificity, we will consider FRET between the electrons belonging to two different NQDs, similarly to what is schematically illustrated in Figure 2.1. It is known that direct (without SP participation) FRET occurs between two NQDs only at very short distances, on the order of just a few nanometres [55-57]. We will be interested in the FRET over larger distances where it occurs predominantly via an SP-mediated process. We assume that the transitions $i \leftrightarrow f$ between the initial and final states in NQDs are unpolarized, i.e. the corresponding transition dipole moments $(\mathbf{d}_d)_{if}$ and $(\mathbf{d}_a)_{if}$ are randomly oriented vectors. In such a case, substituting Hamiltonian (2.27) into the Fermi golden rule and averaging over the dipole orientations, we obtain an expression for the plasmon-enhanced FRET rate γ_F,

$$\gamma_F = \frac{2\pi \left|(\mathbf{d}_d)_{if}\right|^2 \left|(\mathbf{d}_a)_{if}\right|^2}{9\hbar^2} \left|W_{\alpha\beta}(\mathbf{r},\mathbf{r}';\omega)\right|^2 J\,, \tag{2.28}$$

where the dyadic renormalization potential is defined through the renormalized interaction $W(\mathbf{r},\mathbf{r}';\omega)$ [see Eq. (2.7)] as

$$W_{\alpha\beta}(\mathbf{r},\mathbf{r}';\omega) = \frac{\partial^2}{\partial r_\alpha \partial r'_\beta} W(\mathbf{r},\mathbf{r}';\omega)\,,\ \alpha,\beta = x,y,z\,, \tag{2.29}$$

and J is the spectral overlap integral.

Another important process, which can contribute to the linewidths of the NQD donor and acceptor transitions, is the nonradiative transfer of energy from NQDs to a metal. The corresponding contribution to the linewidths γ_m can be found in a straightforward way [26] in the form

$$\gamma_m = -\frac{2\pi|\mathbf{d}|^2}{3\hbar\varepsilon_d} \operatorname{Im} \overline{G}_{\alpha\beta}(\mathbf{r},\mathbf{r};\omega)\,, \tag{2.30}$$

where $\mathbf{d}$ is either $\mathbf{d}_d$ or $\mathbf{d}_a$, $\mathbf{r}$ is the position of the NQD, which is considered as a point-like object, and the dyadic Green's function is defined by Eq. (1.42).

Besides the FRET and the energy transfer to the metal (nonradiative relaxation), there is also the process of the radiative relaxation, which can also be enhanced by the nanoplasmonic system (nanoantenna effect [26]). The corresponding transition renormalized (SP-enhanced) dipole $\mathbf{d}_r$ and the radiative relaxation rate γ_r are given by

$$\gamma_r = \frac{4\omega^3}{3\hbar c^3} \left|\mathbf{d}_r\right|^2,\ d_{r\alpha} = d_\alpha + d_\beta \int_V \Theta(\mathbf{r}') G_{\alpha\beta}(\mathbf{r},\mathbf{r}';\omega) d^3 r'\,. \tag{2.31}$$

where $\mathbf{d}$ is the bare transition dipole.

We will calculate here the FRET rate $\bar{\gamma}_F$ averaged over the position of the acceptor on the nanoshell with inner and outer radii b and a. Because we are interested in the SP-enhanced transfer over distances much exceeding the usual Förster range, we disregard the bare Coulomb potential $V(\mathbf{r}-\mathbf{r}')$. Then substituting the SP eigenfunctions and eigenvalues [see (2.8), (2.9)] into (2.28) and integrating over the solid angle of the vector $\mathbf{r}'$, we obtain [46]

$$\bar{\gamma}_F = \frac{2\pi|\mathbf{d}_d|^2|\mathbf{d}_a|^2}{9\varepsilon_d^2\hbar^2 a^6} J\sum_{l=1}^{\infty}|F_l(x,\omega)|^2(2l+1)(l+1)^2\left(\frac{a^2}{rr'}\right)^{2l+4}. \tag{2.32}$$

The rate γ_m of the excitation quenching due to the energy transfer to the metal on the nanoshell is obtained from (2.30) by the substitution of the SP eigenfunctions and eigenvalues. This procedure is actually greatly simplified, without affecting the result, if the angular averaging is performed. This leads to a simple expression [46]

$$\gamma_m = -\frac{|\mathbf{d}|^2}{6\varepsilon_d\hbar a^3}\sum_{l=1}^{\infty}\mathrm{Im}\,F_l(x,\omega)(2l+1)(l+1)\left(\frac{a}{r}\right)^{2l+4}. \tag{2.33}$$

We compute the FRET rate for CdSe NQDs that are situated at the surface of a silver nanoshell. For certainty, we further assume that they are positioned at the opposite sides of the nanoshell, as illustrated in Figure 2.4(a). In CdSe NQDs the lowest-energy emitting exciton state has a relatively weak oscillator strength and is shifted by a few tens of meV (global Stokes shift) to the red with respect to the stronger absorbing transition (see spectra shown by the bold black lines in Figure 2.4(a)). Because of this significant Stokes shift, the energy transfer occurs with an appreciable efficiency only between NQDs with some size differences, which provides resonant coupling of the emitting state of the donor (the smaller NQD) to the absorbing state of the acceptor (the larger NQD) [56, 57]. This process is schematically illustrated in Figure 2.4 (a).

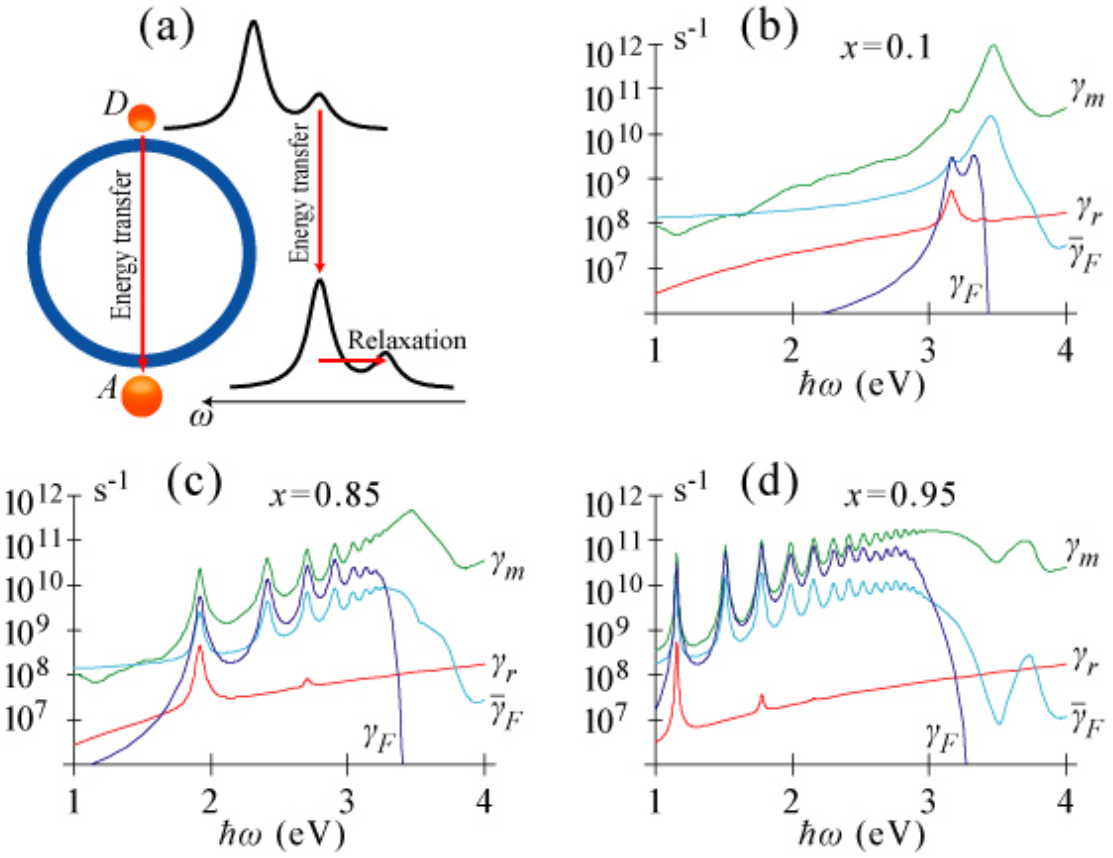

Figure 2.4. (color online) Transfer and relaxation rates for NQDs at the outer surface of a silver nanoshell, modified and enhanced by SPs. (a) Schematic of the system and energy transfer processes. A nanoshell is indicated by a blue circle, and the donor and acceptor NQDs are labeled by *D* and *A*, correspondingly. The frequency distributions of the transition oscillator strengths of the donor and acceptor NQDs are shown by bold black curves. The energy transfer between NQDs and subsequent relaxation are indicated by red arrows. (b)–(d) The nonradiative and radiative relaxation rates (on logarithmic scale) for NQDs on nanoshells for the aspect ratios $x = b/a$ specified in the panels. The FRET rate γ_F (2.28) for two NQDs situated on the opposite poles of a nanoshell (cf. panel (a)) is shown by the blue curves. The SP-mediated FRET rate averaged over the position of the acceptor on the nanoshell $\bar{\gamma}_F$ (2.32) is shown by the light-blue curves. The rate of transfer to the metal γ_m (2.33) is plotted in green. The radiative rate γ_r (2.31) for a NQD at the surface of the nanoshell is depicted by the red curves.

After the Förster energy transfer, indicated by the vertical red arrow, there is a fast (< 1 ps lifetime) relaxation into the lower-frequency state of the acceptor, which precludes energy transfer back to the donor and allows one to use the perturbation theory result of (2.28)

describing an irreversible transfer. We used the adopted NQD parameters for room temperature condition [56]: $J = 0.004$ cm (or 0.13 ps), $d_a = 25$ Debye, and $d_d = 4.4$ Debye.

For certainty, we consider a nanoshell with outer radius $a = 20$ nm. The donor and acceptor NQDs are separated by 2 nm from the metal surface. The FRET rates along with the rates of the nonradiative and radiative decays of the NQDs are displayed in Figure 2.4(b)–(d).We show both the FRET rate γ_F (2.28) for the transfer across the diameter of the nanoshell (dark-blue curves) and the FRET rate $\bar{\gamma}_F$ (2.32) averaged over the random position of the acceptor on the surface of the NQD (light-blue curves). This averaged rate is calculated and shown per single acceptor; if several acceptors participate in the energy transfer, this rate should be multiplied by the number of such acceptors on the nanoshell. Also shown by the green curves is the rate γ_m (2.33) of nonradiative relaxation due to the energy transfer to the metal. The rate of radiative decay, γ_r, (2.31) is depicted by the red curves.

For all aspect ratios (Figure 2.4(b)–(d)), the FRET rates γ_F and $\bar{\gamma}_F$ are enhanced at the frequencies of the SP eigenmodes, which is manifested by the corresponding resonant peaks in the graphs. The number of the efficiently contributing multipoles progressively increases from two (dipole and quadrupole) for a low aspect ratio (x = 0.1, panel (a)) to very many multipoles for high aspect ratios (x = 0.85 - 0.95, panels (c) and (d)). With increasing aspect ratio x, the corresponding FRET rates in these peaks (at the resonant SP frequencies) become higher by orders of magnitude. This FRET transfer rate is especially large in the lower-frequency spectral range, which is due to the higher plasmonic quality of the metal.

The energy transfer to metal is an important process because it competes with FRET. The nonradiative relaxation rate in the donor state of isolated NQDs is low ($< 0.05 \text{ns}^{-1}$); therefore the

energy transfer rate to metal γ_m is the major factor that determines the quantum yield of FRET: $Q_F = \gamma_F / (\gamma_m + \gamma_F)$. We can see from Figure 2.4(b) that for low-aspect ratio nanoshells $\gamma_F << \gamma_m$ and, hence, $Q_F << 1$ implying that the FRET is inefficient. Low efficiency FRET was also found for solid nanospheres [53]. As the aspect ratio increases (panels (c) and (d)), this metal-quenching rate γ_m also shows plasmonic peaks; however, it is enhanced significantly less than the FRET rate. Correspondingly, for x = 0.95 the FRET quantum yield is rather high, $Q_F \sim 0.5$, in the red and near-IR regions of the spectrum. In contrast, the radiative rate γ_r (2.31) is orders of magnitude lower than γ_m; correspondingly, the photoemission quantum yield is very low. Note that the radiative rate is enhanced only in the odd-multipole (dipole, octupole, etc) SP resonances due to the parity selection rule.

The overall conclusion from Figure 2.4 is that the SP renormalization of the Coulomb interaction causes a strong enhancement of the Förster transfer at large distances, across the entire nanoshell and over a wide range of frequencies where many multipole SP resonances contribute. This enhancement is especially pronounced for high-aspect ratio nanoshells in the red and near-IR frequency range where rather high FRET efficiency is predicted.

2.5 General Properties of SP-Renormalized Quasistatic Interaction

To summarize briefly, significant renormalization of the Coulomb interaction between charged particles (electron, holes, and lattice ions) in the vicinity of a plasmonic nanosystem is demonstrated for transitions resonant with SP eigenmodes in the nanosystem. There are three important features of this renormalized interaction $W(\mathbf{r}, \mathbf{r}'; \omega)$ that we have shown above and would like to re-emphasize here. (i) This renormalization (enhancement) is highly resonant. Its

phase depends on the frequency detuning of the electronic transitions with respect to the SP resonant frequency, changing by π (from in-phase to out-of-phase and vice versa) as the frequency ω scans from the red to the blue side of the SP resonance. (ii) The renormalized interaction $W(\mathbf{r},\mathbf{r}';\omega)$ is long-ranged: the effective interaction length is on the order of the size of the entire nanosystem. (iii) This renormalization and plasmonic enhancement of the Coulomb interaction is a universal effect, which should affect a wide range of physical phenomena in the vicinity of the metal nanoplasmonic systems: scattering between charge carriers and the carriers and ions, ion-ion interactions, exciton formation, etc. One of the enhanced and long-range phenomena, which is due to the nanoplasmonic renormalization of the Coulomb interaction, is the Förster energy transfer that becomes efficient for high-aspect ratio nanoshells.

Among other potentially very important applications of this theory are chemical reactions and catalysis on nanostructured metal surfaces. Chemical reactions occur due to the Coulomb interaction between charged particles (electrons and ions) at small distances. In many cases, nanostructured metals, in particular noble metal nanostructures with pronounced plasmonic behavior, are good catalysts. The results of this theory show that the Coulomb interaction at small distances is significantly renormalized. As we have emphasized in the previous paragraph, this renormalization is highly resonant, depending on the frequency ω of a transition that controls the chemical transformation (for example, breaking a chemical bond, establishing a desired new bond, isomerization, etc). This renormalization leads to suppression of the Coulomb interaction for the red detunings from the plasmonic resonance. In contrast, this local interaction is greatly enhanced for blue detunings from the SP resonance. This resonant effect opens up an avenue toward ‘designer’ nanostructured catalysts that can, e.g., favor one specific reaction path over others. Another class of important effects, which are based on the nonlocal nature of the

renormalized Coulomb interaction in the vicinity of a nanoplasmonic system, is the nonlocal (cross) scattering. A charge at some point can undergo a transition, scattering from a charge at a remote position, thus ‘teleporting’ momentum and energy. One important instance of such a remote scattering is a nonlocal SERS where an electronic transition occurs at one point but the vibrational energy is deposited at a distant point of the nanoplasmonic system.

Chapter 3. Electromagnetic Retardation and Surface Plasmon Polaritons (SPPs)

3.1 Retardation Effects

As was described in Sect. 1.1, if the time variation of electromagnetic field is not fast enough to overpower the spatial gradients of the field, then the Maxwell equations dramatically simplify, and electric and magnetic effects can be described separately [1-3, 6]. The formal condition for this simplification to be valid is given by Eqs. (1.16) and (1.18). Quasistatics is extremely relevant for nanoplasmonics and has a broad field of applications as was shown in Chapters 1-2 (see also [22, 26]). Indeed, one of the main goals of nanoplasmonics is to achieve extremely intense localized fields – the LSPs, which are inherently quasistatic [58]. In contrast, electromagnetic fields, which are not as intertwined with matter as LSPs (the ideal example being light in vacuum), do not obey quasistatic approximation. The surface plasmon polaritons (SPPs) represent an intermediate case between radiation in the vacuum and quasistatic LSPs. SPP oscillations include coupling to both the magnetic field and collective oscillations of the solid state electron gas. Retardation effects considered in this Chapter determine the transition between the two extreme cases of vacuum radiation and LSPs. To incorporate the retardation in the electrostatic equations (1.1)-(1.2) one needs to restore the coupling to the magnetic field, as well as to add equations that describe the magnetic field itself. After macroscopic averaging [2, 6] (see also Sect. 1.1) one obtains the system of macroscopic Maxwell differential equations

$$\nabla \cdot \mathbf{D}(\mathbf{r}) = 4\pi\rho_{ext}\,, \tag{3.1}$$

$$\nabla \times \mathbf{E}(\mathbf{r}) = ik_0\mathbf{B}(\mathbf{r})\,, \tag{3.2}$$

$$\nabla \cdot \mathbf{B}(\mathbf{r}) = 0\,, \tag{3.3}$$

$$\nabla \times \mathbf{B}(\mathbf{r}) = -ik_0\mathbf{D}(\mathbf{r}) + (4\pi/c)\mathbf{j}_{ext}\,, \tag{3.4}$$

where $k_0 = (\omega/c)$. In the notations adopted in Eqs. (3.1)-(3.4) the charge distributions that bear no net charge and whose density can be represented by divergence of a vector $\rho_P = -\nabla \cdot \mathbf{P}$, are included in the electric induction $\mathbf{D} = \mathbf{E} + 4\pi\mathbf{P}$. The continuity condition for the motion of these charges is satisfied automatically by the definition (which is already included into Eq. (3.4))

$$\mathbf{j}_P = -i\omega\mathbf{P}\,. \tag{3.5}$$

The continuity condition for external charges, which lead to the net charge, automatically follows from Eqs. (3.1) and (3.4).

We do not consider systems with magnetization, whose introduction is problematic at optical frequencies [6, 59]. Therefore we set $\mathbf{B} = \mathbf{H}$, and below these vectors will be used interchangeably.

The retardation enters into the system (3.1)-(3.4) through the term on the right-hand side of Eq. (3.2), which leads to circulation of electric field generated by magnetic flux, and through the displacement current $\mathbf{j}_D = -i\omega\mathbf{D}(\mathbf{r})/4\pi$ present in Eq. (3.4).

Consider a homogeneous region with dielectric permittivity ε free from external charges. Using equations (3.2) and (3.4) one can obtain wave equation for electric field

$$\nabla \times \nabla \times \mathbf{E}(\mathbf{r}) - k_0^{\,2}\varepsilon\mathbf{E}(\mathbf{r}) = 0\,, \tag{3.6}$$

and similar one for magnetic field. Since in this case $\nabla \cdot \mathbf{E}(\mathbf{r}) = 0$ (see Eq. (3.1)), Eq. (3.6) can be rewritten as a Helmholtz equation

$$\nabla^2 \mathbf{E}(\mathbf{r}) + k_0{}^2 \varepsilon \mathbf{E}(\mathbf{r}) = 0\,, \tag{3.7}$$

leading to dispersion relation for electromagnetic waves within a homogeneous region [2, 6]

$$k^2 = k_0{}^2 \varepsilon\,, \tag{3.8}$$

where **k** is the wavevector of the electromagnetic wave. Solutions in different regions of homogeneity should be matched by conditions given by Eqs. (1.9), (1.10), whose form is not changed by the retardation effects. Other conditions follow from Eqs. (3.3) and (3.4) [2, 6]

$$(\mathbf{B}_{out} - \mathbf{B}_{in}) \cdot \mathbf{n} = 0\,, \tag{3.9}$$

$$\mathbf{n} \times (\mathbf{B}_{out} - \mathbf{B}_{in}) = \frac{4\pi}{c} \mathbf{K}\,, \tag{3.10}$$

where **K** is the surface current density at the boundary between two regions of homogeneity.

3.2 Radiative Decay of SPs

The properties of LSP resonances depend on the dephasing rate γ (see Sect. 1.2). Theoretically expression (1.31) becomes invalid for nanoparticles with radii $R \geq l_s \approx 25\,\mathrm{nm}$, since it is derived by means of the quasistatic approximation. Besides the quasistatic decay rate contribution, LSPs on large nanoparticles decay radiatively. The LSP radiative decay has been investigated in many different metal nanostructures both experimentally and numerically [30, 32, 60]. There is no general analytical representation of LSP radiative lifetime, due to absence of full electrodynamic spectral theory of LSPs (see Refs. [61, 62]) similar to the quasistatic spectral theory described in [19] (see Sect. 1.2). This is related to the fact that the problem of electromagnetic LSP resonances is reminiscent of the quantum mechanical problem of quasi-discrete states [63], which is not a proper eigenproblem [64]. Despite of this fact, we were able to

derive a general expression for the radiative decay rate here for the first time, bypassing these difficulties.

Let us consider a two-component structure, of the same type as in Sect. 1.2. Let the field $\mathbf{E}(\mathbf{r},t)=\mathbf{E}_0(\mathbf{r})e^{-\gamma t}e^{-i\omega t}$ be a solution to Maxwell equations (3.1)-(3.4) (with no external charges) inside some volume V, enclosed by surface S. This field should satisfy the following equations:

$$\Theta(\mathbf{r})\mathbf{E}_0(\mathbf{r})-s(\Omega)\left(\mathbf{E}_0(\mathbf{r})-\frac{\nabla\times\nabla\times\mathbf{E}_0(\mathbf{r})}{k^2\varepsilon_d}\right)=0,\ \nabla\times\mathbf{E}_0(\mathbf{r})=ik\mathbf{H}_0(\mathbf{r}), \tag{3.11}$$

where complex frequency $\Omega=\omega-i\gamma$, $k=\Omega/c$, $s(\omega)=\left[1-\varepsilon_m(\omega)/\varepsilon_d\right]^{-1}$ is the spectral parameter and $\Theta(\mathbf{r})$ is the geometric function, which is equal to 1 in the metal and 0 in the dielectric. From Eq. (3.11), using vector identities, we obtain

$$\int_V\Theta(\mathbf{r})\left|\mathbf{E}_0\right|^2dV=s(\Omega)\left(\int_V\left|\mathbf{E}_0\right|^2dV+\frac{\left|k\right|^2}{k^2\varepsilon_d}\int_V\left|\mathbf{H}_0\right|^2dV+\frac{i}{k\varepsilon_d}\oint_S(\mathbf{E}_0^*\times\mathbf{H}_0)\cdot\hat{\mathbf{n}}\,dS\right), \tag{3.12}$$

where $\hat{\mathbf{n}}$ is a normal ort to the surface *S*.

From Eq. (3.12) one can obtain an expression for imaginary part of inverse of the spectral parameter $1/s(\Omega)$ to be

$$\mathrm{Im}\left(\frac{1}{s(\Omega)}\right)\int_V\Theta(\mathbf{r})\left|\mathbf{E}_0\right|^2dV=\left(-\frac{2\omega\gamma}{\varepsilon_d\left|\Omega\right|^2}\int_V\left|\mathbf{H}_0\right|^2dV+\oint_S\mathrm{Re}\left(\frac{\mathbf{E}_0^*\times\mathbf{H}_0}{k\varepsilon_d}\right)\cdot\hat{\mathbf{n}}\,ds\right), \tag{3.13}$$

Acting in the same manner as in (1.28) and neglecting terms on the order of Q^{-1} for the dephasing rate we obtain

$$\gamma=\frac{\mathrm{Im}\,\varepsilon_m(\omega)}{\mathrm{Re}\dfrac{\partial\varepsilon_m}{\partial\omega}}+\frac{1}{\mathrm{Re}\dfrac{\partial\varepsilon_m}{\partial\omega}}\frac{\oint_S\mathrm{Re}\left(\mathbf{E}_0^*\times\mathbf{H}_0\right)\cdot\hat{\mathbf{n}}\,ds}{k_0\int_V\Theta(\mathbf{r})\left|\mathbf{E}_0\right|^2dV}. \tag{3.14}$$

The first term in Eq. (3.14) represents the quasistatic dephasing [19, 20, 27] (see Eq. (1.31)), while the second term is the radiative decay rate, which can be also represented in terms of cycle-averaged quantities as

$$\gamma_r = \frac{1}{\mathrm{Re}\dfrac{\partial \varepsilon_m}{\partial \omega}} \frac{4\pi}{\omega} \frac{\oint_S \overline{\mathbf{S}} \cdot \hat{\mathbf{n}}\, ds}{\int_V \Theta(\mathbf{r}) \overline{\mathbf{E}}^2 dV}. \tag{3.15}$$

where $\overline{\mathbf{S}}$ is the time-averaged Poynting vector.

Consider a radiative decay of a dipole nanoparticle. The intensity of dipole radiation is given by [6]

$$I = \oint_S \overline{\mathbf{S}} \cdot \hat{\mathbf{n}}\, ds = \frac{4\omega^4 \varepsilon_d^{1/2}}{3c^3} |\mathbf{d}|^2. \tag{3.16}$$

The dipole moment of a small spherical nanoparticle is given by

$$\mathbf{d} = \frac{\varepsilon_m - \varepsilon_d}{4\pi} \int \Theta(\mathbf{r}) \overline{\mathbf{E}} dV \approx \frac{\varepsilon_m - \varepsilon_d}{4\pi} V \overline{\mathbf{E}} = \frac{\varepsilon_m - \varepsilon_d}{3} R^3 \overline{\mathbf{E}}. \tag{3.17}$$

Substituting this into (3.15), combined with the condition for dipole resonance of the nanoparticle, $\varepsilon_m = -2\varepsilon_d$ we obtain

$$\gamma_r = \frac{4\varepsilon_d^{5/2}}{\mathrm{Re}\dfrac{\partial \varepsilon_m}{\partial \omega}} \left(\frac{\omega R}{c} \right)^3. \tag{3.18}$$

This result coincides with expression obtained earlier for dipole radiative decay rate using the pole approximation for quantum polarizability [65]. Note that quasistatic decay rate (the first term in Eq. (3.14), see also Eq. (1.31)) dominates the LSP dephasing even for radii larger than l_s. For gold the ratio $\gamma_r / \gamma_{st} \approx 4(k_0 R)^3 / \mathrm{Im}\, \varepsilon_m$ comes close to unity at $R_{rad} \approx 70$ nm at SP resonance, while for silver this critical radius is $R_{rad} \approx 25\,\mathrm{nm}$ [65].

LSP radiative decay is extremely important in plasmonics [30, 32, 60]. Expression (3.15) describes radiative decay for any solution of Maxwell equations in two-component structures and, in principle, can serve as a tool in LSP radiative decay engineering.

3.3 SPPs at Planar Surfaces

Consider a metal-dielectric boundary (plane $z = 0$, metal being in the $z < 0$ half-space) and a wave with frequency ω incident upon it from the dielectric side with wavevector in the plane *xz* and angle of incidence θ. The metal dielectric function is denoted as $\varepsilon_m(\omega)$, while the dielectric permittivity of the dielectric is ε_d. The presence of the boundary splits the incident wave into transmitted and reflected waves [2, 6]. It is important that there are two independent cases of this separation depending on whether the magnetic field is perpendicular to the plane of incidence (TM polarization), or the electric field is (TE polarization). We consider the situation of the TM-polarized incident wave that is more important for us. We will write the magnetic fields of the waves as

$$\mathbf{H}_\alpha(r,t) = \hat{\mathbf{y}} H_\alpha e^{ik_{\alpha x}x} e^{ik_{\alpha z}z} e^{-i\omega t}, \tag{3.19}$$

where $\alpha = i, r, t$ denotes incident, reflected and transmitted fields correspondingly. The problem is translationally invariant in the *xy* plane. Therefore, the field dependence on these coordinates should be the same in both media, which leads to the phase matching condition for all three waves

$$k_{ix} = k_{rx} = k_{tx} = k_x = k_0 \sqrt{\varepsilon_d} \sin\theta, \tag{3.20}$$

From Eqs. (3.8) and (3.20) it follows that *z*-components have the form

$$k_{iz} = -k_{rz} = -\sqrt{k_0^2 \varepsilon_d - k_x^2}\,, \tag{3.21}$$

$$k_{tz} = -\sqrt{k_0^2 \varepsilon_m(\omega) - k_x^2} = i\kappa_m\,. \tag{3.22}$$

Metal dielectric functions in plasmonics, i.e. $\varepsilon_m(\omega)$ at frequencies between near-infrared and visible range, are almost real negative numbers. Therefore, expression (3.22) is almost imaginary and the field exponentially decays into the metal. The length of this decay is the so-called skin depth (see Sect. 1.1) given by

$$l_s = 1/\mathrm{Re}\,\kappa_m = \frac{\lambda\!\!\!^{-}_0}{\mathrm{Re}\sqrt{-\varepsilon_m(\omega) + \varepsilon_d \sin^2\theta}}\,. \tag{3.23}$$

The skin depth reaches maximum at normal incidence, where it depends only on the metal dielectric function (see Eq. (1.17) and Figure 1.1). The skin depth for non-zero incidence angles differs from the estimate (1.17) by $1-3\,\mathrm{nm}$ (if incidence is from vacuum).

As follows from boundary conditions, the amplitudes of the reflected and transmitted magnetic fields are connected to that of the incident field through the Fresnel coefficients r_{TM}, t_{TM} [6]

$$H_r = \frac{\varepsilon_m k_{iz} - \varepsilon_d k_{tz}}{\varepsilon_m k_{iz} + \varepsilon_d k_{tz}} H_i = r_{TM} H_i\,, \tag{3.24}$$

$$H_t = \frac{2\varepsilon_m k_{iz}}{\varepsilon_m k_{iz} + \varepsilon_d k_{tz}} H_i = t_{TM} H_i\,, \tag{3.25}$$

The Fresnel coefficients have a pole which corresponds to the surface resonance

$$\varepsilon_m k_{iz} + \varepsilon_d k_{tz} = 0\,. \tag{3.26}$$

The index of refraction $n = k_x/k_0$ for the surface resonance can be found [6, 25, 26, 66] from Eqs. (3.21), (3.22) and (3.26) as:

$$n(\omega) = \sqrt{\frac{\varepsilon_m(\omega)\varepsilon_d}{\varepsilon_m(\omega) + \varepsilon_d}}\,. \tag{3.27}$$

Condition (3.26) and the corresponding index of refraction represent a mode that can sustain itself without energy flux from the incident wave (see Eqs. (3.24) and (3.25)). Moreover, in the particular configuration we consider here, the incident wave becomes unphysical and should be excluded, as it is explained below. Instead, the SPP wave should be excited from the $x \to -\infty$ side (in the selected notations) of the boundary plane (see the next Section). This mode is called the surface plasmon polariton (SPP). It is a physically well-defined excitation, if $\mathrm{Re}\, n(\omega) >> \mathrm{Im}\, n(\omega)$. This situation normally occurs at the metal-vacuum interface below the frequency of static surface plasmon $\omega_{SP} \approx \omega_p / \sqrt{2}$, where ω_p is the metal plasma frequency. This plasma frequency is on the order of several electronvolts for most metals. Below the plasma frequency the real part of metal dielectric function is negative $\mathrm{Re}[\varepsilon_m(\omega)] < 0$. From this fact and from Eq. (3.27) follows the condition for SPP existence, given by

$$\mathrm{Re}[\varepsilon_m(\omega)] \le -\varepsilon_d\,. \tag{3.28}$$

The dispersion of metal dielectric permittivity is described very well by the Drude formula

$$\varepsilon_m(\omega) = \varepsilon_b - \frac{\omega_p^2}{\omega(\omega + i\gamma)}\,. \tag{3.29}$$

where ε_b is background dielectric permittivity which can be contributed, for example, by phonons, and γ is the inverse of the electron relaxation time. With the Drude formula taken into consideration, Eq. (3.28) translates into condition $\omega \le \omega_p / \sqrt{\varepsilon_b + \varepsilon_d}$.

Substituting Eq. (3.27) into Eqs. (3.21) and (3.22) one obtains the transverse distribution of the field in an SPP [26]

$$k_{rz} = k_0\sqrt{\varepsilon_d - n^2} = ik_0\sqrt{-\frac{\varepsilon_d^2}{\varepsilon_m(\omega)+\varepsilon_d}} = i\kappa_d\,, \tag{3.30}$$

$$k_{tz} = -k_0\sqrt{\varepsilon_m(\omega) - n^2} = -ik_0\sqrt{-\frac{\varepsilon_m^2(\omega)}{\varepsilon_m(\omega)+\varepsilon_d}} = -i\kappa_m\,, \tag{3.31}$$

where the decrements κ_m and κ_d are almost real positive numbers, whose small imaginary parts come from the metal absorption. The fact that in a SPP wave k_{rz} and k_{tz} are imaginary means that SPP propagation is restricted to a direction along the metal-dielectric boundary (the *x*-axis in our notation) and SPP field decays exponentially away from the boundary. The SPP skin depth is again determined by κ_m as

$$l_s = 1/\mathrm{Re}\,\kappa_m = \frac{\lambda_0}{\mathrm{Re}\sqrt{-\varepsilon_m^2(\omega)/(\varepsilon_m(\omega)+\varepsilon_d)}}. \tag{3.32}$$

Additionally the penetration length into dielectric is usually defined for SPPs as

$$l_d = 1/\mathrm{Re}\,\kappa_d = \frac{\lambda_0}{\mathrm{Re}\sqrt{-\varepsilon_d^2/(\varepsilon_m(\omega)+\varepsilon_d)}}. \tag{3.33}$$

While the SPP field is evanescent, or exponentially decays from the boundary, the field of the incident wave under SPP existence conditions exponentially diverges at large distances from the boundary. This field does not correspond to any physical incident wave and should be excluded. Electromagnetic waves propagating toward a metal surface cannot satisfy the phase matching condition (3.20) with an SPP field on the metal-dielectric boundary. In other words SPP cannot be excited directly by illuminating a smooth planar metal surface by electromagnetic radiation, since linear momentum is not conserved in such a process. There are several conventional ways of SPP excitation that are discussed in the next Section.

3.4 Excitation of SPPs

To excite SPP waves one needs to fulfill both energy and momentum conservation. As we have shown in the previous Section, SPPs on a planar interface are dark modes and cannot be excited by, nor can they decay into photons, due to larger momentum of the SPPs at a given energy. One way to excite an SPP is to use a grating coupler. The excitation is achieved due to additional momentum coming from a reciprocal lattice vector of the grating, so that the new wave-vector is $k'_{ix} = k_{ix} + 2\pi m/a$, where a is the grating period [67-72]. A grating on the metal surface was the setting for the first observation of SPPs by Wood [73]. The grating coupling of SPP to radiation has been first used to experimentally determine the dispersion relation of the SPPs on a metal-dielectric interface [74]. Periodic perforation of flat surfaces of ideal metals with grooves or holes allows not only the excitation of SPPs for further propagation along flat surfaces, but also leads to the appearance of surface electromagnetic waves in perfect conductors. These mimic ("spoof") SPPs are much more strongly bound to the surfaces than conventional SPPs in far-infrared [75-77]. The perforation of metals has been used to enhance the interaction of subwavelength holes and slits in metal films with SPPs [78-81].

Another well-known method to increase light momentum is by using a dielectric with permittivity larger than unity. In this case the wavevector is increased by the factor of $\sqrt{\varepsilon_d}$, which allows for an SPP excitation by an attenuated total reflection method. This has been achieved by Otto [82] and by Kretschmann and Raether [83]. Both the Otto and Kretschmann geometries use dielectric prisms to increase light momentum. In the Otto geometry the prism is not contacting the metal surface and in the air gap between them evanescent fields are created through total internal reflection in the prism [84, 85]. These fields excite SPPs on the metal

surface. In the Kretschmann geometry the prism contacts a metal film surface directly and SPPs are excited on the opposite side of the film by the evanescent fields [85, 86].

Similarly SPPs can be excited locally, if the metal boundary is placed near a source of confined optical near fields that have wave-vector components parallel to the boundary and that satisfy phase matching conditions with SPPs. Subwavelength apertures, fluorescent molecules or metallic particles and others can serve as such sources of confined fields [24, 26, 87].

Historically one of the first methods by which SPPs were excited was transmission of high-energy electrons through metal films [88]. One can observe losses in the spectrum of transmitted electrons due to SPP excitation. Electron energy loss spectra (EELS) represent a powerful method to study SPP properties [89].

3.5 SPPs and SPs at Metal Nanowires

It has been shown experimentally that metal nanowires support SPP modes and are able to guide optical energy over several microns [90, 91]. SPPs in metal nanowires are very important for modern technology [92]. Besides subwavelength guiding, the small sizes of the metal nanowires lead to strong coupling between nanowires and individual quantum emitters [93, 94]. Metal nanowires support azimuthally symmetric SPP mode at all wire radii, which allows gradual concentration of optical energy via such SPPs in adiabatically tapered nanowires [95, 96], creating extremely strong (up to metal breakdown) and highly localized fields, crucial for modern technology.

Consider a metal nanowire with radius R and dielectric permittivity $\varepsilon_m(\omega)$ embedded into a dielectric matrix with dielectric constant ε_d. A propagating SPP with frequency ω creates surface charge densities both from the metal and dielectric sides of the interface. The charge

density in dielectric or metal is given by $\rho_{d,m}(\mathbf{r}) = \frac{1}{2\pi}\sigma_{d,m}(z)\delta(\rho - R)$ with corresponding Fourier components $\rho_{d,m}(\boldsymbol{\kappa}) = \sigma_{d,m}(k)RJ_0(qR)$, where the wavevector is $\boldsymbol{\kappa} = k\hat{\mathbf{z}} + q\hat{\boldsymbol{\rho}}$, with $\hat{\mathbf{z}}$ and $\hat{\boldsymbol{\rho}}$ being orts of a cylindrical coordinate system. Using the Maxwell equations (3.1)-(3.4) we obtain expressions for the complex amplitudes of the azimuthally symmetric mode (TM_0)

$$\mathbf{E}_\omega = \begin{cases} -\frac{2i\sigma_m}{\varepsilon_m}(\kappa_m R)K_0(\kappa_m R)\left(\frac{\kappa_m}{k}I_0(\kappa_m\rho)\hat{\mathbf{z}} - iI_1(\kappa_m\rho)\hat{\boldsymbol{\rho}}\right), \rho < R \\ -\frac{2i\sigma_d}{\varepsilon_d}(\kappa_d R)I_0(\kappa_d R)\left(\frac{\kappa_d}{k}K_0(\kappa_d\rho)\hat{\mathbf{z}} + iK_1(\kappa_d\rho)\hat{\boldsymbol{\rho}}\right), \rho > R \end{cases}, \tag{3.34}$$

$$\mathbf{H}_\omega = \begin{cases} -2\sigma_m\frac{k_0}{k}(\kappa_m R)K_0(\kappa_m R)I_1(\kappa_m\rho)\hat{\boldsymbol{\varphi}}, \rho < R \\ 2\sigma_d\frac{k_0}{k}(\kappa_d R)I_0(\kappa_d R)K_1(\kappa_d\rho)\hat{\boldsymbol{\varphi}}, \rho > R \end{cases}, \tag{3.35}$$

where $\kappa_m = \sqrt{k^2 - k_0^2\varepsilon_m}$, $\kappa_d = \sqrt{k^2 - k_0^2\varepsilon_d}$ and k is the SPP wavenumber. Complex fields resulting from (3.34)-(3.35) are proportional to $e^{-i\omega t}$.

Matching tangential components of the fields (3.34)-(3.35) leads to the following relationships

$$\frac{\sigma_m\kappa_m^2}{\varepsilon_m}K_0(\kappa_m R)I_0(\kappa_m R) = \frac{\sigma_d\kappa_d^2}{\varepsilon_d}I_0(\kappa_d R)K_0(\kappa_d R), \text{ and} \tag{3.36}$$

$$-\sigma_m\kappa_m K_0(\kappa_m R)I_1(\kappa_m R) = \sigma_d\kappa_d I_0(\kappa_d R)K_1(\kappa_d R).$$

Excluding surface charges from the system (3.36), we arrive at the SPP characteristic equation

$$-\frac{\kappa_m}{\varepsilon_m}\frac{I_0(\kappa_m R)}{I_1(\kappa_m R)} = \frac{\kappa_d}{\varepsilon_d}\frac{K_0(\kappa_d R)}{K_1(\kappa_d R)}. \tag{3.37}$$

An important SPP property is its energy flux, which is given by the averaged over an SPP oscillation period Poynting vector:

$$\overline{\mathbf{S}} = \frac{c}{4\pi}\overline{\mathbf{E}\times\mathbf{H}} = \frac{c}{8\pi}e^{-2\,\mathrm{Im}[k]z}\,\mathrm{Re}(\mathbf{E}\times\mathbf{H}^*). \tag{3.38}$$

Using the expressions for the fields (3.34)-(3.35) which we have obtained for the TM_0 SPP mode we calculate the Poynting vector as

$$\overline{S_z} = \frac{c}{8\pi} e^{-2\,\mathrm{Im}[k]z}\,\mathrm{Re}\begin{cases} \dfrac{4|\sigma_m|^2}{\varepsilon_m}\dfrac{k_0}{k^*}\left|(\kappa_m R)K_0(\kappa_m R)I_1(\kappa_m \rho)\right|^2, \rho < R \\ \dfrac{4|\sigma_d|^2}{\varepsilon_d}\dfrac{k_0}{k^*}\left|(\kappa_d R)I_0(\kappa_d R)K_1(\kappa_d \rho)\right|^2, \rho > R. \end{cases} \tag{3.39}$$

Expression (3.39) allows a computation of the time averaged flux of SPP energy (input power) through a plane $z = 0$ as

$$\mathscr{P} = 2\pi \int_0^\infty \rho d\rho \overline{S_z}(z=0) \tag{3.40}$$

Computation of (3.40) requires the following facts [49, 97]

$$\left[I_1(z)\right]^* = I_1(z^*),\ \left[K_1(z)\right]^* = K_1(z^*), \tag{3.41}$$

$$\int xI_p(ax)I_p(bx)dx = \frac{x}{a^2-b^2}\left(aI_p(bx)I_{p+1}(ax) - bI_p(ax)I_{p+1}(bx)\right). \tag{3.42}$$

Relations (3.41)-(3.42) can be combined to obtain

$$\int xI_p(ax)I_p(a^*x)dx = \frac{x}{a^2 - a^{*2}}\left(aI_p(a^*x)I_{p+1}(ax) - a^*I_p(ax)I_{p+1}(a^*x)\right) = \tag{3.43}$$

$$= \frac{x\,\mathrm{Im}[aI_p(a^*x)I_{p+1}(ax)]}{2\,\mathrm{Re}[a]\,\mathrm{Im}[a]} = \frac{x\,\mathrm{Im}[aI_p(a^*x)I_{p-1}(ax)]}{2\,\mathrm{Re}[a]\,\mathrm{Im}[a]}.$$

Finally, for the input power (3.40), we have

$$\mathscr{P} = c|\sigma_m|^2 R^2 \Theta_{R\omega}, \tag{3.44}$$

where

$$\Theta_{R\omega} = \mathrm{Re}\left[\frac{k_0}{\varepsilon_m k^*}\right]\left|(\kappa_m R)K_0(\kappa_m R)\right|^2 \frac{\mathrm{Im}[\kappa_m I_1(\kappa_m{}^* R)I_0(\kappa_m R)]}{2R\cdot\mathrm{Re}[\kappa_m]\,\mathrm{Im}[\kappa_m]} + \tag{3.45}$$

$$+ \frac{\varepsilon_d{}^2|\kappa_m|^4}{|\varepsilon_m|^2|\kappa_d|^4}\left|\frac{K_0(\kappa_m R)I_0(\kappa_m R)}{K_0(\kappa_d R)I_0(\kappa_d R)}\right|^2 \mathrm{Re}\left[\frac{k_0}{\varepsilon_d k^*}\right]\left|(\kappa_d R)I_0(\kappa_d R)\right|^2 \frac{\mathrm{Im}[\kappa_d K_1(\kappa_d{}^* R)K_0(\kappa_d R)]}{2R\cdot\mathrm{Re}[\kappa_d]\,\mathrm{Im}[\kappa_d]}.$$

The first part of Eq. (3.36) in the form $\sigma_d = \sigma_m \dfrac{\varepsilon_d \kappa_m{}^2}{\varepsilon_m \kappa_d{}^2}\dfrac{K_0(\kappa_m R)I_0(\kappa_m R)}{K_0(\kappa_d R)I_0(\kappa_d R)}$ was used to obtain (3.45).

Now the components of electromagnetic field (3.34), (3.35) in an SPP pulse can be represented as follows

$$\mathbf{E} = A(t')(\widetilde{E}_z\hat{\mathbf{z}} + \widetilde{E}_\rho\hat{\boldsymbol{\rho}})e^{i(kz-\omega t)},\ \mathbf{H} = A(t')\widetilde{H}_\varphi\hat{\boldsymbol{\varphi}}e^{i(kz-\omega t)} \tag{3.46}$$

where $t' = t - z/v_g$, v_g is the SPP group velocity at the pulse carrier frequency ω, k is the SPP wave number and functions $\widetilde{E}_z$, $\widetilde{E}_\rho$ and $\widetilde{H}_\varphi$ depend only on radius ρ:

$$\widetilde{E}_z = \begin{cases} -\dfrac{2i}{\varepsilon_m\sqrt{c\Theta_{R\omega}}}\dfrac{\kappa_m^{\,2}}{k}K_0(\kappa_m R)I_0(\kappa_m\rho), \rho < R \\ -\dfrac{2i}{\varepsilon_m\sqrt{c\Theta_{R\omega}}}\dfrac{\kappa_m^{\,2}}{k}\dfrac{I_0(\kappa_m R)}{K_0(\kappa_d R)}K_0(\kappa_m R)K_0(\kappa_d\rho), \rho > R \end{cases} \tag{3.47}$$

$$\widetilde{E}_\rho = \begin{cases} -\dfrac{2\kappa_m}{\varepsilon_m\sqrt{c\Theta_{R\omega}}}K_0(\kappa_m R)I_1(\kappa_m\rho), \rho < R \\ \dfrac{2\kappa_m}{\varepsilon_m\sqrt{c\Theta_{R\omega}}}\dfrac{\kappa_m}{\kappa_d}\dfrac{I_0(\kappa_m R)}{K_0(\kappa_d R)}K_0(\kappa_m R)K_1(\kappa_d\rho), \rho > R \end{cases} \tag{3.48}$$

$$\widetilde{H}_\varphi = \begin{cases} -\dfrac{2\kappa_m}{\sqrt{c\Theta_{R\omega}}}\dfrac{k_0}{k}K_0(\kappa_m R)I_1(\kappa_m\rho), \rho < R \\ \dfrac{2\kappa_m}{\sqrt{c\Theta_{R\omega}}}\dfrac{k_0}{k}\dfrac{\varepsilon_d\kappa_m}{\varepsilon_m\kappa_d}\dfrac{I_0(\kappa_m R)}{K_0(\kappa_d R)}K_0(\kappa_m R)K_1(\kappa_d\rho)\hat{\boldsymbol{\varphi}}, \rho > R. \end{cases} \tag{3.49}$$

We select the normalization for the real amplitude $A(t)$ to satisfy the relation $A^2(t) = \mathscr{P}(t)$. Disregarding the group velocity dispersion in Eq. (3.46) is valid for pulses with duration of tens of femtoseconds and greater, and frequencies not too close to the SP resonance [98].

Let us consider the limit of extremely thin wires $R << l_s$, where l_s is the skin depth of the metal nanowire. To describe this situation consider the limit when $k >> k_0\sqrt{|\varepsilon_m|}, k_0\sqrt{\varepsilon_d}$. In this case $\kappa_m, \kappa_d \approx k$ and the SPP dispersion equation (3.37) can be approximated by

$$\xi(x) = \frac{I_0(x)}{I_1(x)}\frac{K_1(x)}{K_0(x)} = -\frac{\varepsilon_m(\omega)}{\varepsilon_d},\ x = kR. \tag{3.50}$$

One can resolve Eq. (3.50) for the wavevector

$$k = \frac{x}{R} = \frac{1}{R}\xi^{-1}(-\varepsilon_m(\omega)/\varepsilon_d)\,. \tag{3.51}$$

As can be seen from Figure 3.1 the approximation (3.51) works very well for thin nanowires. The solutions satisfy $x = kR \approx 1$, which in conjunction with $k >> k_0\sqrt{|\varepsilon_m|}$ gives $R << l_s$. This limit is very significant for plasmonics since sub-skin-depth metal nanowires (adiabatically tapered) are one of the structures where concentration of optical energy on the nanoscale can be achieved [95].

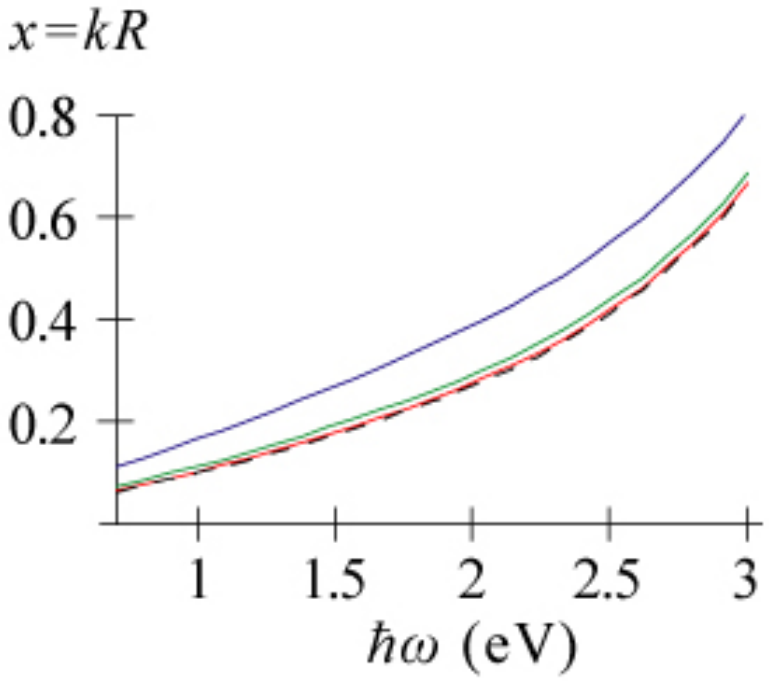

Figure 3.1. (color online) Real part of the parameter $x = kR$ for an SPP in silver nanowire in vacuum as a function of frequency $\hbar\omega$ for exact solution of Eq. (3.37), when $R = 5\,\text{nm}$ (red), $R = 10\,\text{nm}$ (green), $R = 25\,\text{nm}$ (blue) and for quasi-static solution of Eq. (3.51) (broken black curve). The quasi-static solution approximates exact solutions with $R << l_s \approx 25\,\text{nm}$ (see Figure 1.1) extremely well.

Chapter 4. Forces in Electromagnetic Fields

4.1 Introduction

In 1619 Kepler hypothesized that tails of comets are deflected from the Sun due to mechanical pressure of solar radiation [26, 99]. Later Maxwell's theory of electromagnetic radiation has shown that radiation carries momentum and correspondingly can transfer it to matter [100]. The numerical value of light pressure due to incident radiation upon a surface, which is normal to the light propagation direction is given by expression [26]

$$p = W_0(1 + R)\,, \tag{4.1}$$

where W_0 is electromagnetic energy density in the incident wave and R is the reflection coefficient of the surface. The pressure changes from W_0 for a black surface to $2W_0$ for an ideally reflecting surface. The value of this pressure is extremely small, which has made it very difficult to measure the effect of radiation pressure. Nevertheless, it was first measured in experiments by Lebedew [101]. Lebedew's results agreed with the Maxwell's theory, which was important evidence in favor of this theory. Lebedew's studies have also showed there would be substantial effect of light pressure on macroscopic particles in the interstellar medium, partially confirming the Kepler hypothesis.

In 1905 Einstein proposed the concept of the photon ("das Lichtquant") [102] following the suggestion by Max Plank that energy exchange between light and matter occurs in discrete quanta [103]. In 1909 Einstein suggested the existence of light pressure fluctuations associated

with emission or absorption of quanta with discrete values of momentum [104]. In 1925 Compton experimentally demonstrated the discrete momentum transfer between X-rays and electrons [105]. In 1933 the deflection of a beam of sodium atoms by the light pressure from a sodium lamp was observed by Frisch [106]. This deflection was extremely weak, far below the magnitudes at which it could have any practical application.

The invention of the laser changed the prospects of radiation pressure applications, creating several huge fields based on momentum transfer from light to matter. The action of laser radiation upon micron-sized particles and neutral atoms was first investigated in the 1970s in works of Ashkin [107, 108] and Letokhov [109]. Ashkin and his collaborators have proposed to trap atomic particles using focused laser beams. Presently such optical tweezers allow trapping and manipulation of macroscopic particles and even living cells in the range of sizes from 0.1 to 10 micrometers [110-112].

Another important application of light-matter momentum transfer, which became possible with invention of the laser, is laser cooling [113]. This effect takes place if the radiation frequency is tuned to the red of an electronic transition in the particles to be cooled. Due to the Doppler effect, the atoms absorb more photons if they move toward the light source. In a laser cooling experiment two lasers irradiate particles from opposite directions and particles always absorb more photons from the source pointing opposite to their direction of motion. Acquiring more momentum from the direction opposite to the motion of the particle means decreasing the velocity of the particle. This leads to the cooling effect.

The advent of high-power lasers and appearance of high-power radiation fluxes have made practical another effect based on light-matter interaction: the photon drag effect. Light propagating through a semiconductor gets absorbed and transfers its momentum to

semiconductor charge carriers. This effect was first observed by Danishevskii et al. [114] and Gibson et al. [115]. The photon drag effect became of great technical importance for infrared and terahertz detection of picosecond pulses using semiconductor photon drag detectors [116].

4.2 Electromagnetic Stress-Energy Tensor

For a system with Lagrangian $\Lambda\left(q, \frac{\partial q}{\partial x_i} \equiv q_i\right)$ one can introduce a tensor [1]

$$T_i^k = q_i \frac{\partial \Lambda}{\partial q_k} - \Lambda \,, \tag{4.2}$$

for which the relationship

$$\frac{\partial T_i^k}{\partial x^k} = 0 \tag{4.3}$$

is satisfied. Here q is some function of spatial coordinates and time (denoted as x_i, with $i = 0$ for time), which determines the state of the system. Relation (4.3) is equivalent to the statement that the following vector is conserved

$$P^i = \frac{1}{c}\int T^{ik} dS_k \,, \tag{4.4}$$

where the integration is over a hypersurface containing a three-dimensional space. The vector given by (4.4) is the 4-momentum of the system, and T^{ik} is the stress-energy tensor. It has to be symmetric, with $T^{ik} = T^{ki}$.

If we select for integration in (4.4) the hypersurface $x^0 = const$ the 4-momentum assumes the following form

$$P^i = \frac{1}{c}\int T^{i0} dV \,, \tag{4.5}$$

where now the integration is over the 3-dimensional space. The space components of P^i form the 3-momentum of the system, while the temporal component is its energy divided by c. Therefore, the momentum density of the system is given by

$$\mathbf{p} = \frac{1}{c}\left(T^{10}, T^{20}, T^{30}\right), \tag{4.6}$$

and energy density by

$$W = T^{00}. \tag{4.7}$$

From Eq. (4.3) it follows that energy flux density, $\mathbf{S} = c^2\mathbf{p}$, is connected to momentum density W. Other components of the tensor form a 3-tensor $-\sigma_{\alpha\beta}$ $(\alpha, \beta = x, y, z)$ of momentum flux density or the stress tensor with inverse sign.

The electromagnetic Lagrangian [1]

$$\Lambda = -\frac{1}{16\pi} F_{kl} F^{kl}, \tag{4.8}$$

leads to the following expression for electromagnetic stress-energy tensor

$$T^{ik} = \frac{1}{4\pi}\left(-F^{il}F_l^{\ k} + \frac{1}{4} g^{ik} F_{lm} F^{lm}\right), \tag{4.9}$$

In expressions (4.8), (4.9) F^{kl} is the tensor of electromagnetic field and g^{ik} is the metric tensor.

The electromagnetic 3-dimensional stress tensor, called the Maxwell tensor, can be expressed in terms of electric and magnetic fields [1-3]

$$\begin{aligned} \sigma_{\alpha\beta} &= \frac{1}{4\pi}\left(E_\alpha E_\beta + H_\alpha H_\beta - \frac{1}{2}\delta_{\alpha\beta}(E^2 + H^2)\right) = \\ &= \frac{1}{4\pi}\left(\mathbf{E}\otimes\mathbf{E} + \mathbf{H}\otimes\mathbf{H} - \frac{1}{2}(E^2 + H^2)\hat{\mathbf{I}}\right)_{\alpha\beta} \end{aligned} \tag{4.10}$$

where $\otimes$ denotes outer vector product which gives tensor $(\mathbf{B}\otimes\mathbf{A})_{ik} = B_i A_k$ and $\hat{\mathbf{I}}$ is a unity matrix.

4.3 Energy and Momentum Transfer in Electromagnetic Fields

It can be shown that stress-energy tensor is directly connected to energy and momentum transfer between electromagnetic field and electric charges in this field. Indeed, considerations of the Maxwell equations (3.1)-(3.4) taken in the temporal domain in the vacuum, i.e. when $\mathbf{D} = \mathbf{E}$ and $\mathbf{B} = \mathbf{H}$, shows that [1]

$$\begin{aligned} \operatorname{div}\mathbf{S} &= \operatorname{div}\left[\frac{c}{4\pi}(\mathbf{E}\times\mathbf{H})\right] = \frac{c}{4\pi}\left\{(\nabla\times\mathbf{E})\cdot\mathbf{H} - (\nabla\times\mathbf{H})\cdot\mathbf{E}\right\} \\ &= \frac{c}{4\pi}\left[-\frac{1}{c}\frac{\partial\mathbf{H}}{\partial t}\cdot\mathbf{H} - \frac{1}{c}\frac{\partial\mathbf{E}}{\partial t}\cdot\mathbf{E} - \frac{4\pi}{c}\mathbf{j}_{ext}\cdot\mathbf{E}\right] = -\frac{\partial}{\partial t}\left(\frac{E^2+H^2}{8\pi}\right) - \mathbf{j}_{ext}\cdot\mathbf{E} \end{aligned} \tag{4.11}$$

Here $\mathbf{S} = \frac{c}{4\pi}(\mathbf{E}\times\mathbf{H})$ is the Poynting vector, which is electromagnetic energy flux. The term $\mathbf{j}_{ext}\cdot\mathbf{E}$ is the change of the kinetic energy of the charges in an electromagnetic field, i.e. the energy transferred from an electromagnetic field to charges, and it is expressed in terms of stress-energy tensor elements:

$$\mathbf{j}_{ext}\cdot\mathbf{E} = -\left(\frac{\partial W}{\partial t} + \operatorname{div}\mathbf{S}\right) \tag{4.12}$$

Similarly, momentum transfer can be determined from stress-energy tensor elements [26]

$$\begin{aligned} &\frac{\partial}{\partial t}\left(\frac{\mathbf{S}}{c^2}\right) = \frac{1}{4\pi c}\left(\frac{\partial\mathbf{E}}{\partial t}\times\mathbf{H} + \mathbf{E}\times\frac{\partial\mathbf{H}}{\partial t}\right) = \\ &= \frac{1}{4\pi}\left((\nabla\times\mathbf{H})\times\mathbf{H} + (\nabla\times\mathbf{E})\times\mathbf{E}\right) - \frac{1}{c}(\mathbf{j}_{ext}\times\mathbf{H}) + \frac{\nabla\cdot\mathbf{E}}{4\pi}\mathbf{E} - \rho_{ext}\mathbf{E} = \\ &= \operatorname{div}\left[\frac{1}{4\pi}\left(\mathbf{E}\otimes\mathbf{E} + \mathbf{H}\otimes\mathbf{H} - \frac{1}{2}(E^2+H^2)\hat{\mathbf{I}}\right)\right] - \rho_{ext}\mathbf{E} - \frac{1}{c}(\mathbf{j}_{ext}\times\mathbf{H}) \end{aligned} \tag{4.13}$$

Here the following identity has been used

$$\left[(\nabla\times\mathbf{A})\times\mathbf{B} + \mathbf{A}(\nabla\cdot\mathbf{B})\right]_k = \partial_i(B_iA_k) - B_i\partial_kA_i = \left\{\operatorname{div}\left(\mathbf{B}\otimes\mathbf{A} - (\mathbf{B}^c\cdot\mathbf{A})\hat{\mathbf{I}}\right)\right\}_k, \tag{4.14}$$

where superscript “c” exempts a vector from differentiation.

Eq. (4.13) expresses the change of momentum of external charges in electromagnetic field, given by the Lorentz force $\mathbf{F}_{ext} = \rho_{ext}\mathbf{E} + \frac{1}{c}(\mathbf{j}_{ext} \times \mathbf{H})$, through the elements of the stress-energy tensor:

$$\mathbf{F}_{ext} = -\left[\frac{\partial}{\partial t}\left(\frac{\mathbf{S}}{c^2} \right) - \nabla \cdot \hat{\boldsymbol{\sigma}} \right] \tag{4.15}$$

Consider, for example, an electromagnetic wave in the vacuum, incident and partially reflected from some interface. The field in front of the interface has the following form

$$\begin{aligned} \mathbf{E} &= \hat{\mathbf{x}} E_0 \,\mathrm{Re}\left(e^{ikz} + re^{-ikz} \right) e^{-i\omega t} \\ \mathbf{H} &= \hat{\mathbf{y}} E_0 \,\mathrm{Re}\left(e^{ikz} - re^{-ikz} \right) e^{-i\omega t} \end{aligned} \tag{4.16}$$

The pressure exerted by the wave (4.16) can be computed using Eq. (4.15) as [26]

$$p\hat{\mathbf{z}} = \frac{1}{A}\int_A \overline{\hat{\boldsymbol{\sigma}}} \cdot \hat{\mathbf{z}}\, ds = \hat{\mathbf{z}} W_0 \left(1 + |r|^2 \right), \quad W_0 = \frac{E_0^2}{4\pi} \tag{4.17}$$

where A is an area on the surface parallel to the interface and $\overline{\hat{\boldsymbol{\sigma}}}$ is time averaged stress tensor. Eq. (4.17) is consistent with Eq. (4.1). The idea behind this example was generalized by Novotny for compute forces acting on dielectric particles in optical tweezers using expression similar to (4.17), but with integration over surfaces enclosing corresponding particles [111].

4.4 Forces Acting on a Dipole in an Electromagnetic Field

To better understand the components contributing to force in electromagnetic fields, for example, in optical tweezers, let us consider the force acting on an electric dipole in an electromagnetic field. The dipole $\mathbf{d}$ is situated at point $\mathbf{r}$. Charges of the dipole experience a Lorentz force

$$\mathbf{F}_q(\mathbf{r}) = q\left[\mathbf{E}(\mathbf{r}) + \frac{1}{c}\dot{\mathbf{r}} \times \mathbf{B}(\mathbf{r}) \right]. \tag{4.18}$$

The resultant force on the dipole is given by

$$\mathbf{F} = \mathbf{F}_q\left(\mathbf{r} - \frac{\mathbf{d}}{2q}\right) + \mathbf{F}_{-q}\left(\mathbf{r} + \frac{\mathbf{d}}{2q}\right). \tag{4.19}$$

Expanding over $\mathbf{d}/q$ to the first order we obtain [117]

$$\mathbf{F} = (\mathbf{d}\cdot\nabla)\mathbf{E} + \frac{1}{c}\dot{\mathbf{d}}\times\mathbf{B} + \frac{\dot{\mathbf{r}}}{c}\times(\mathbf{d}\cdot\nabla)\mathbf{B} \tag{4.20}$$

We drop the last term, since we assume that $\dot{\mathbf{r}}/c << 1$. We can rearrange the second term as follows

$$\frac{1}{c}\dot{\mathbf{d}}\times\mathbf{B} = \mathbf{d}\times\left(-\frac{1}{c}\frac{\partial\mathbf{B}}{\partial t}\right) + \frac{1}{c}\frac{d}{dt}(\mathbf{d}\times\mathbf{B}) = \mathbf{d}\times(\nabla\times\mathbf{E}) + \frac{1}{c}\frac{d}{dt}(\mathbf{d}\times\mathbf{B}) \tag{4.21}$$

Here we used the fact that $d\mathbf{B}/dt \approx \partial\mathbf{B}/\partial t$, since $\dot{\mathbf{r}}/c << 1$. This gives an expression for the force

$$\mathbf{F} = \nabla(\mathbf{d}^c\cdot\mathbf{E}) + \frac{1}{c}\frac{d}{dt}(\mathbf{d}\times\mathbf{B}), \tag{4.22}$$

where the following identity was utilized

$$(\mathbf{A}\cdot\nabla)\mathbf{B} + \mathbf{A}\times(\nabla\times\mathbf{B}) = \nabla(\mathbf{A}^c\cdot\mathbf{B}); \tag{4.23}$$

as in Eq. (4.14) the superscript "c" exempts a vector from differentiation.

Let us consider a monochromatic field

$$\mathbf{E} = \mathrm{Re}\ \mathbf{E}_0(\mathbf{r})e^{-i\omega t},\ \mathbf{B} = \mathrm{Re}\ \mathbf{B}_0(\mathbf{r})e^{-i\omega t} \tag{4.24}$$

The dipole moment in this field assumes the following form

$$\mathbf{d} = \mathrm{Re}\ \mathbf{d}_0 e^{-i\omega t},\ \mathbf{d}_{\circ} = \alpha(\omega)\mathbf{E}_0(\mathbf{r}), \tag{4.25}$$

where $\alpha(\omega)$ denotes the dipole polarizability.

The time averaged force in field (4.24) is given by

$$\overline{\mathbf{F}} = \frac{1}{2}\mathrm{Re}\nabla(\mathbf{d}_0\cdot\mathbf{E}_0^{\ *}) \tag{4.26}$$

Representing the complex amplitude as $\mathbf{E}_0 = E_R e^{i\varphi_R}\hat{\mathbf{n}}$, where $\mathbf{E}_R$ and φ_R are real, and $\hat{\mathbf{n}}$ gives the field's polarization, we get [26]

$$\overline{\mathbf{F}} = \frac{1}{2}\mathrm{Re}\left\{\alpha\left(E_R\nabla E_R - iE_R^2\nabla\varphi_R\right)\right\} = \frac{\alpha'}{4}\nabla E_R^2 + \frac{\alpha''}{2}E_R^2\nabla\varphi_R\,. \tag{4.27}$$

where we used the usual notation $\alpha = \alpha' + i\alpha''$. The first term in Eq. (4.27) is the striction (or gradient) force, while the second one is the pressure force.

Consider a focused laser beam. A small dielectric particle in this beam is acted upon by two forces, according to (4.27). In the direction of the light beam propagation there is the light pressure force on the particle, while striction force pulls the particle into the region of high intensity, i.e. towards the focus. This principle is behind so-called optical tweezers, which allow control and manipulation in space of tiny particles by focused light beams.

4.5 Radiation Pressure in Macroscopic Bodies and the Photon Drag Effect

It is difficult to derive an expression for the force acting on distributed object similar to (4.27) (see the next Section), but for the large objects one can neglect the striction force and consider only pressure, since gradients of the fields are not very large in this case. Pressure force density can be nicely estimated as follows. The field energy dissipation per unit of time and per unit of volume Q divided by $\hbar\omega$ is the number of absorbed photons. If this quantity is multiplied by photon momentum $\hbar\mathbf{k}$, we obtain the rate of momentum transfer from radiation to matter per unit volume, or the pressure force density

$$\mathbf{f}_p = \frac{Q}{\hbar\omega}\hbar\mathbf{k} = \frac{\omega\varepsilon''}{8\pi}E^2\frac{\mathbf{k}}{\omega} = \frac{\chi''}{2}\mathbf{k}E^2\,. \tag{4.28}$$

Expression (4.28) is the same as the second term in (4.27) with the imaginary part of the macroscopic polarizability χ'', instead of the dipole polarizability α''.

An extremely important practical application of radiation pressure is the photon drag effect in semiconductors [115]. Consider a light beam with intensity P in watts propagating through a semiconductor. The average rate of momentum transfer due to absorption from the beam to the sample per unit volume is

$$\frac{P}{c} e^{-\alpha L} \frac{\alpha}{A}, \tag{4.29}$$

where α is the semiconductor absorption coefficient (cm^{-1}), L is the distance into the sample and A is the cross-section of the sample perpendicular to the beam. This momentum transfer drive the free carriers along the sample, but in the case of an open circuit it leads to the emergence of a rectified field E opposing the pressure force. This is the photon drag effect. The photon drag field at the depth L is given by

$$neE = \frac{P}{c} e^{-\alpha L} \frac{\alpha}{A}, \tag{4.30}$$

where n is electron density. To obtain the total open circuit rectified voltage one should integrate (4.30) over the whole sample, with the length denoted as L_0 [115]:

$$V = -\frac{P(1-R)}{Anec} \frac{1-e^{-\alpha L_0}}{1+R\cdot e^{-\alpha L_0}} \approx R_H \frac{P}{A}(1-R), \tag{4.31}$$

Here reflection, with coefficient R on both sides of the sample, is taken into account and $R_H = -1/(nec)$ is the Hall constant. The last part of the equation (4.31) is correct if the sample is long or if absorption is strong, so that $\alpha L_0 >> 1$.

4.6 Macroscopic Force Acting on Polarized Matter

In a recent paper [118] we have derived a general formula describing momentum transfer between electromagnetic fields and extended polarizable structures. Consider a metal

nanostructure propagating an SPP pulse. The SPP field produces polarization $\mathbf{P}$, charges with macroscopic density $\rho = -\operatorname{div}\mathbf{P}$, current density $\mathbf{j} = \partial\mathbf{P}/\partial t$, and surface charge density $\sigma = (\mathbf{P}\cdot\mathbf{n})$ at the surface of the metal, where $\mathbf{n}$ is the normal to the surface pointing outward. We do not consider systems with optical magnetism, whose introduction at optical frequency is problematic [6, 59]. Therefore $\mathbf{B} = \mathbf{H}$, which precludes the existence of surface currents.

Then a macroscopic (averaged) Lorentz force density inside the material volume is given by

$$\mathbf{f}_v = -\mathbf{E}(\nabla\cdot\mathbf{P}) + \frac{1}{c}\frac{\partial\mathbf{P}}{\partial t}\times\mathbf{B}\,. \tag{4.32}$$

The surface polarization charges experience the Lorentz force with a surface density

$$\mathbf{f}_s = \sigma\mathbf{E}\,. \tag{4.33}$$

Using relation (4.14) the volume force density given by Eq. (4.32) can be represented in the following way

$$\begin{aligned}\mathbf{f}_v &= -\nabla\cdot(\mathbf{P}\otimes\mathbf{E}) + \nabla(\mathbf{P}^c\cdot\mathbf{E}) + (\nabla\times\mathbf{E})\times\mathbf{B} + \frac{1}{c}\frac{\partial\mathbf{P}}{\partial t}\times\mathbf{B} = \\ &= -\operatorname{div}(\mathbf{P}\otimes\mathbf{E}) + \operatorname{grad}(\mathbf{P}^c\cdot\mathbf{E}) + \frac{1}{c}\frac{\partial(\mathbf{P}\times\mathbf{B})}{\partial t}\end{aligned}\,, \tag{4.34}$$

Thus, the total force acting on the polarization charges in the SPP field is

$$\mathbf{F} = \int_V \mathbf{f}_v dV + \oint_S \mathbf{f}_s ds\,, \tag{4.35}$$

where the first integration runs over volume V of the structure, and the second is over its surface S. Noticing that the volume integral of the first term in the last part of Eq. (4.34) is equal to

$$-\int_V \operatorname{div}(\mathbf{P}\otimes\mathbf{E})dV = -\oint_S (\mathbf{P}\cdot\mathbf{n})\mathbf{E}ds = -\oint_S \mathbf{f}_s ds\,, \tag{4.36}$$

we cancel terms in Eq. (4.35) to simplify it and obtain the following general expression for the time-averaged total force acting upon the object [118]

$$\overline{\mathbf{F}} = \frac{1}{2}\mathrm{Re}\int_V \left(\mathrm{grad}(\mathbf{P}^c \cdot \mathbf{E}^*) + \frac{1}{c}\frac{\partial(\mathbf{P}\times\mathbf{B}^*)}{\partial t} \right) dV\,, \tag{4.37}$$

Note that we calculate macroscopic forces assuming that the nanostructure is homogeneous enough and the frequencies under consideration are far enough from the surface plasmon (SP) resonances. Then the field fluctuations, characteristic of the disordered systems [4], can be disregarded.

The result (4.37) is of fundamental importance for processes involving interaction of nanoplasmonic fields with metal electrons. Equation (4.37) is similar to the force acting on a point dipole moment (see Eq. (4.22) and Ref. [117]), but is more general. It is valid for a wide range of problems with a general material equation $\mathbf{P} = \hat{\chi}\mathbf{E}$, including those where operator $\hat{\chi}$ describes anisotropic or non-local media. The first term in Eq. (4.37) includes the pressure and gradient (striction) forces similarly to Eq. (4.27), which is extremely important for nanotechnology, since the gradient (striction) force becomes large on the nanoscale (see Chapter 5). The second term in Eq. (4.37) is known as the Abraham force. In a monochromatic field, this force averaged over the period of oscillations is zero, but in the field of a pulsed excitation it has a finite magnitude.

Chapter 5. Giant Surface Plasmon-Induced Drag Effect (SPIDEr)

5.1 Introduction

The fact that electromagnetic fields exert mechanical forces on matter is well known and has found applications in atomic physics [109, 113] and bio- and nanotechnology [110, 111, 119], and picosecond photodetectors based on the photon drag effect (PDE) [116]. The semiconductor PDE detectors have proved to be very practical for relatively fast detection of picosecond pulses in a wide frequency range spanning from THz to infrared. It has been proposed to use enhanced fields in phonon-polariton silicon carbide structures for laser particle accelerators [120]. There have been experimental investigations of the PDE in metal nanofilms that are thicker than the skin depth [121, 122]. Metals support surface plasmon polaritons (SPPs) [66] that exert forces on electrons causing an SPP-enhanced PDE [121]. However, the PDE is typically rather small, with the induced potential differences in the mV range. This modest enhancement of the PDE in these experiments was due to relatively slow variation of SPP fields in space, and the momentum transferred to the electrons was correspondingly small. Because of the long relaxation times of the SPPs at plane metal surfaces, this PDE is also expected to be relatively slow. A drag effect under the conditions of strong nanoplasmonic confinement, when the SPP localization radius is less than the skin depth ($\sim$ 25 nm), has not been studied or exploited theoretically or experimentally.

In the paper [118] we have proposed a giant surface plasmon induced drag effect (SPIDEr) in metal nanowires which is fast, with a response on the femtosecond time scale. We

show that the ultrashort, nanolocalized SPP pulses exert forces on electrons in the nanowires, inducing giant THz electromotive force (emf) along the SPP propagation direction [see schematic in Figure 5.1].

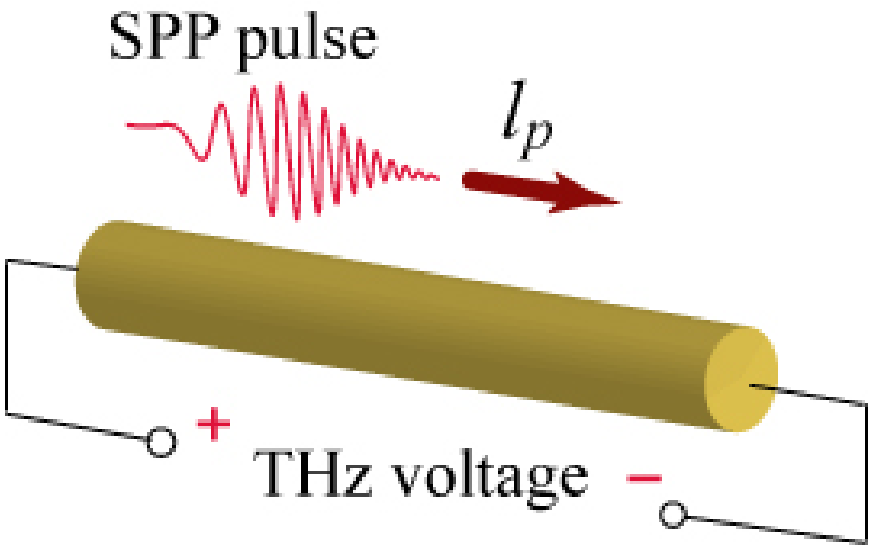

Figure 5.1. (color online) Schematic of a SPIDEr in metal nanowire. Propagating SPPs create forces acting on carriers in the nanowire, which leads to THz-band voltage (emf) between the ends of the wire. Picosecond or femtosecond pulses can be used to manipulate the time dependence of the created emf.

We have found that in thin (~ 5 nm radius) wires this emf can reach ~ 10 V, with nanolocalized THz fields as high as ~ 1 MV/cm. Such THz field have previouisly been generated in the far zone [123], where they produce non-perturbative effects [124], but not on the nanoscale. In contrast, the plasmonic metal nanowires can serve as nanolocalized sources of high THz fields. We also study the dynamics of the SPIDEr for short SPP pulses and suggest that thin metal nanowires can be used as broadband nanoscopic photodetectors with extremely fast response due to the femtosecond momentum relaxation times in metals. The nature of the giant enhancement of the SPIDEr is novel in nanoplasmonics: it is not the enhancement of the optical fields per se (the maximum magnitude of the local fields is limited by the breakdown at the metal surface that occurs for fields ~ 1 V/Å) but the very high gradients of these fields. The SPIDEr is ultrafast

because it is a non-resonant effect whose bandwidth is comparable to that of the entire optical spectrum.

5.2 SPIDEr in Metal Nanowires

We apply the general Eq. (4.37) to describe the SPIDEr. To be specific, consider a metal nanowire with radius R and dielectric susceptibility $\chi(\omega)$, which is oriented along the *z*-axis and embedded in a dielectric with a dielectric permittivity of ε_d. This wire propagates an SPP pulse, which can be excited by external sources using, e.g., the effect of adiabatic compression [95, 96].

In the case of extreme nanoplasmonic confinement ($R << l_s$, where l_s is the skin depth), R becomes the only relevant quantity of the dimensionality of length [95]. Therefore there is scaling of all magnitudes in R. The SPP wave power $\mathscr{P}$ scales as $\mathscr{P} \sim E^2 R^2 v_g$, where $v_g \sim \omega R$ is the SPP group velocity. The SPIDEr-induced potential difference [electromotive force (emf)] $\mathscr{E}$ is proportional to the pressure produced by the force from (4.37), $\mathscr{E} \sim F/E^2$. The propagation length of the SPP, $l_p \sim RQ$, where Q is the SPP figure of merit, independent of R. These arguments allow us to predict scaling of the SPIDEr force F, emf $\mathscr{E}$, and the electric field due to SPIDEr rectification E_R (which for femtosecond SPP pulses possesses THz frequencies): $F \propto \mathscr{P} R^{-1}$, $\mathscr{E} \propto \mathscr{P} R^{-3}$, $E_R \propto \mathscr{P} R^{-4}$, $E_{mR} \propto R^{-1}$. We have also indicated the scaling of the maximum rectified field E_{mR} (at the maximum tolerable power $\mathscr{P}$). The scaling implies that all the effects caused by the SPIDEr increase with decrease in the wire radius as its powers. This enhancement is not resonant and therefore has bandwidth comparable to that of the entire optical spectrum. The scaling describes only the dependence on R. There are also

prefactors describing the dependence on dielectric permittivities, frequency, etc. They take into account an additional enhancement close to the SP resonant frequency, which is multiplicative in magnitude. Below in this chapter we show that this scaling is reproduced by the theory results.

The SPPs are transverse magnetic (TM) modes, and their complex fields have the form (see Sect. 3.5)

$$\mathbf{E} = A(t')(\widetilde{E}_z\hat{\mathbf{z}} + \widetilde{E}_\rho\hat{\boldsymbol{\rho}})e^{i(kz-\omega t)},\ \mathbf{H} = A(t')\widetilde{H}_\varphi\hat{\boldsymbol{\varphi}}e^{i(kz-\omega t)} \tag{5.1}$$

where $t' = t - z/v_g$, v_g is the SPP group velocity at the pulse carrier frequency ω, an k is the SPP wave number. The total power flowing through the plane $z = 0$ at the moment t is $\mathscr{P}(t) = 2\pi\int_0^\infty \rho d\rho \overline{S}_z(\mathbf{r},t)\big|_{z=0}$, where $\overline{S}_z(\mathbf{r},t) = (c/8\pi)\,\mathrm{Re}\left[\mathbf{E}\times\mathbf{H}^*\right]$ is the Poynting vector averaged over the SPP period. Considering the azimuthally symmetric (TM_0) modes, the functions $\widetilde{E}_z$, $\widetilde{E}_\rho$ and $\widetilde{H}_\varphi$ depend only on radius ρ. We normalize them for real amplitude $A(t)$ to satisfy a relation $A^2(t) = \mathscr{P}(t)$. Disregarding the group velocity dispersion in Eq. (5.1) is valid for pulses with duration of tens of femtoseconds and greater, and frequencies not too close to the SP resonance [98].

The momentum transferred from the electromagnetic field to the electronic system implies forces exerted on the electrons. The density of these forces is given by Eqs. (4.32) and (4.33). These forces lead to an emf, which corresponds to optical rectification in the system, which for femtosecond SPP pulses results in the emf in the THz frequency range. Since the electron momentum-relaxation time is on the scale of femtoseconds, electrons come to a local equilibrium in the process of this rectification. Therefore, we will describe it in the hydrodynamic approximation, for which the pressure p and electrostatic potential ϕ satisfy an equation $p + ne\phi = const$, where e is electron charge, and n is electron density. From this

equation, we can find the emf $\mathscr{E} = \Delta\phi$, which is the total change of potential in the direction of SPP propagation (the z direction), $\mathscr{E} = -\Delta p/(ne)$, where $\Delta p = \overline{F}_z/(\pi R^2)$ is the full change of the pressure. Here, $\overline{F}_z$ is z-component of the force (4.37) averaged over the period of SPP oscillations.

Now let us calculate the force $\overline{F}_z$ in the fields given by (5.1)

$$\begin{aligned}
&\overline{F}_z = \frac{1}{2}\mathrm{Re}\int_V (\widetilde{P}_z\widetilde{E}_z^{\,*} + \widetilde{P}_\rho\widetilde{E}_\rho^{\,*})\cdot\left\{-ik\mathscr{P}(t') + \frac{1}{2}\frac{\partial\mathscr{P}(t')}{\partial z}\right\}\cdot e^{-2k''z}\cdot dV = \\
&= \frac{1}{2}\mathrm{Re}\int_V \chi\left|\widetilde{E}\right|^2\cdot\left\{-ik\mathscr{P}(t') + \frac{1}{2}\frac{\partial\mathscr{P}(t')}{\partial z}\right\}\cdot e^{-2k''z}\cdot dV = \\
&= \frac{1}{2}\int_V\left\{\mathrm{Im}(k\chi)\cdot\mathscr{P}(t') + \frac{\chi'}{2}\frac{\partial\mathscr{P}(t')}{\partial z}\right\}\left|\widetilde{E}\right|^2 e^{-2k''z}\cdot dV = \\
&= \left(\pi k'\chi''\int dz\cdot\mathscr{P}(t')e^{-2k''z} + \pi\chi'\int dz\cdot\left\{k''\mathscr{P}(t') + \frac{1}{2}\frac{\partial\mathscr{P}(t')}{\partial z}\right\}\cdot e^{-2k''z}\right)\cdot\int_0^R\left|\widetilde{E}\right|^2\rho d\rho = \\
&= \left(\pi l_p k'\chi''\mathscr{T}(t) - \frac{\pi\chi'}{2}\mathscr{P}(t')\right)\cdot\int_0^R\left|\widetilde{E}\right|^2\rho d\rho = \left(\frac{\pi\chi''Q}{2}\mathscr{T}(t) - \frac{\pi\chi'}{2}\mathscr{P}(t)\right)\cdot\int_0^R\left|\widetilde{E}\right|^2\rho d\rho,
\end{aligned} \tag{5.2}$$

where the integration was accomplished in the following way

$$\begin{aligned}
&\int dz\cdot\left\{k''\mathscr{P}(t') + \frac{1}{2}\frac{\partial\mathscr{P}(t')}{\partial z}\right\}\cdot e^{-2k''z} = \\
&= k''\int dz\cdot\mathscr{P}(t')\cdot e^{-2k''z} + \frac{1}{2}\int dz\cdot\frac{\partial(\mathscr{P}(t')\cdot e^{-2k''z})}{\partial z} - \frac{1}{2}\int dz\cdot\mathscr{P}(t')\frac{\partial e^{-2k''z}}{\partial z} = \\
&= \frac{1}{2}\left(\mathscr{P}(t')\cdot e^{-2k''z}\right)\Big|_{z=0}^{z=\infty} = -\frac{\mathscr{P}(t)}{2},
\end{aligned} \tag{5.3}$$

and a new function was defined via

$$\mathscr{T}(t) = \frac{1}{l_p}\int_0^\infty dz\cdot\mathscr{P}(t')e^{-z/l_p} = \frac{e^{-t/t_p}}{t_p}\int_{-\infty}^{t} dt'\cdot\mathscr{P}(t')e^{-t'/t_p}\ . \tag{5.4}$$

The total force $\overline{F}_z = f_{pr} + f_{st} + f_A$ is composed of three forces: the SPP pressure, striction, and the Abraham force, whose z-components are, correspondingly,

$$f_{pr} = \frac{\pi R^2}{cA_{pr}} \mathscr{T}(t), \; f_{st} = \frac{\pi R^2}{cA_{st}} \mathscr{P}(t), \; f_A = \frac{\pi R^2}{c^2 L_A} \mathscr{T}'(t). \tag{5.5}$$

In Eq. (5.5), coefficients A_{pr} and A_{st} have dimensionality of area, and L_A has dimensionality of length. They are defined as

$$A_{pr} = \left(\frac{c\chi'' Q}{2R^2} \int_0^R \widetilde{E}^2 \rho d\rho \right)^{-1}, \; A_{st} = -\left(\frac{c\chi'}{2R^2} \int_0^R \widetilde{E}^2 \rho d\rho \right)^{-1}, \tag{5.6}$$

$$L_A = \left(\frac{cl_p}{R^2} \int_0^R \mathrm{Re}\left(\chi \widetilde{E}_\rho \widetilde{H}_\varphi^* \right) \rho d\rho \right)^{-1},$$

where $Q = \mathrm{Re}\, k / \mathrm{Im}\, k$ is the SPP figure of merit, $\widetilde{E}^2 = \left| \widetilde{E}_z \right|^2 + \left| \widetilde{E}_\rho \right|^2$, $l_p = 1/(2\,\mathrm{Im}\, k)$ is the SPP propagation length, and $t_p = l_p / v_g$ is the SPP pulse lifetime.

These three forces result in three terms of the SPIDEr emf [118]

$$\mathscr{E}(t) = R_H \left(\frac{\mathscr{T}(t)}{A_{pr}} + \frac{\mathscr{P}(t)}{A_{st}} + \frac{\mathscr{P}'(t)}{cL_A} \right), \tag{5.7}$$

where $R_H = -1/nec$ is the Hall constant (cf. Eq. (4.31)).

The Abraham force contribution [the third term in Eq. (3)] is small under the condition $k_0 l_p / kc\tau << 1$, where $k_0 = \omega / c$, and τ is the pulse duration. This condition is well satisfied for the parameters used in this paper.

We will consider two limiting cases pertaining to Eq. (5.7): a quasi-monochromatic regime of long pulses $\tau >> t_p$ and a regime of short pulses $\tau << t_p$, where t_p is the SPP dissipation time.

5.3 SPIDEr as a THz Source

Consider first the quasi-monochromatic regime ($\tau >> t_p$), where $\mathscr{T}(t) \approx \mathscr{P}(t)$ (see Eq. (5.4)). In such a case, the total emf $\mathscr{E}(t)$ follows the pulse-envelope time dependence $\mathscr{P}(t)$. The computations will be made for a silver [13] nanowire embedded in vacuum ($\varepsilon_d = 1$).

For the quasi-monochromatic case, the total emf $\mathscr{E}$ as a function of frequency ω and wire radius R is displayed in Figure 5.2(a). In contrast to the case of dielectric media, in the present plasmonic case the SPP pressure and striction contributions to the emf have the same sign since $\chi' < 0$. These two contributions are equal if a condition $\chi'' Q < \chi'$ is satisfied. The black solid line represents this condition; to the left of this line the pressure dominates, and to the right the striction force gives the major contribution to the SPIDEr. This is understandable because close to the SP resonance of the wire (at ~ 3.7 eV), the gradient of the SPP intensity increases due to the high loss: the striction force is of a gradient nature, therefore dominating. Similarly, with the decrease of R, the intensity gradient increases due to the increased confinement, which also leads to the relative increase of the striction with respect to the pressure force, as we clearly can see from this and other panels of Figure 5.2. General increase of the SPIDEr at the SP resonant frequency can be seen as a broad red peak.

Magnitude of the SPIDEr emf relative to the SPP wave power, $\mathscr{E}/\mathscr{P}$, is illustrated in Figure 5.2(b) as a function of the wire radius R for a frequency of $\omega = 2.9\,\mathrm{eV}$. The SPIDEr effect is gigantically enhanced for strong nanoplasmonic confinement: by four orders of magnitude when R decreases from 100 to 5 nm at the same SPP power. There is a pronounced scaling $\mathscr{E}/\mathscr{P} \propto R^{-3}$ at $R << l_s$, in accord with the discussion in the beginning of Sect. 5.2.

The spectral dependence of the relative SPIDEr emf, $\mathscr{E}/\mathscr{P}$, for a wire of the smallest radius considered, $R = 5\,\text{nm}$, is depicted in Figure 5.2(c). For significantly thinner wires, nonlocal-response effects may become significant, cf. Refs. [8], [9]. Importantly, the magnitude of the emf in this case is very large, from 0.01 to 10 V per 1 W of the SPP pulse power, in the entire optical range, with a pronounced resonance at the SP frequency. This large magnitude shows that the SPIDEr effect can be used for the photodetection on the nanoscale, i.e., in the role that previously was deemed only available for semiconductors. In this sense, it belongs to the area of active nanoplasmonics [98].

By nonlinear optics classification, the SPIDEr is an optical second-order nonlinear effect: the magnitude of the SPIDEr emf $\mathscr{E}$ is proportional to the power $\mathscr{P}$ of the SPP field. Therefore, the maximum achievable magnitude of the emf is determined by the maximum $\mathscr{P}$ that the wire can tolerate. This we estimate setting the optical field E at the surface of the wire equal to 1 V/Å [125, 126]. For fields significantly higher than this, there will be massive ionization and damage of the metal surface. We plot in Figure 5.2(d) this maximum intensity as a function of the wire radius for three SPP frequencies. Note a very good scaling, $\mathscr{P}_m \propto R^3$, in the region $R \le l_s$ of strong nanoplasmonic confinement. These values of the $\mathscr{P}_m$ in comparison to the data of Figure 5.2(a)-(c) show that the gigantic values of of the SPIDEr emf $\mathscr{E} \sim 10V$ are realistically achievable, which are many orders of magnitude greater than observed previously in the metal films [121, 122].

One of the most important for applications properties of the giant SPIDEr is the high local electric field E_R generated due to the SPIDEr optical rectification near the metal nanowire. Such field (averaged over the SPP decay length l_p) can be found as $E_R = \mathscr{E}/l_p$. We display the

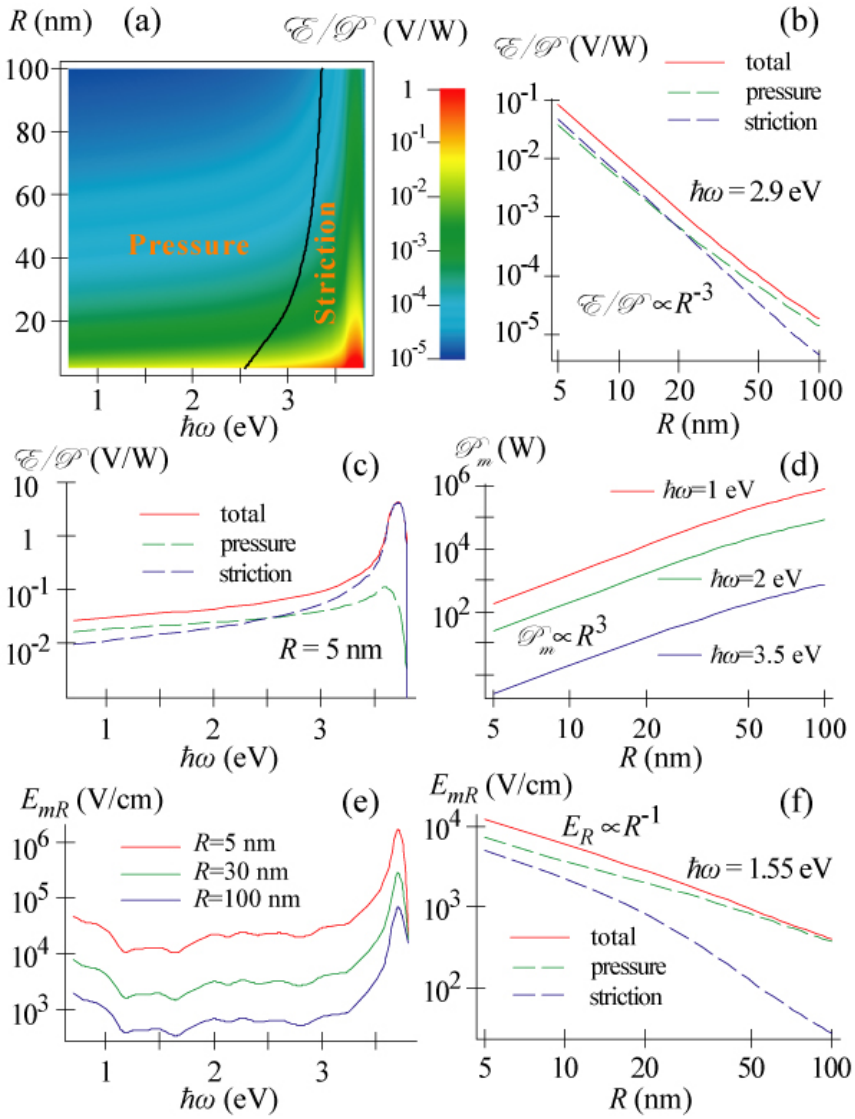

Figure 5.2. (color online) SPIDEr for quasi-monochromatic SPP pulses: emf and rectified field dependence on the frequency $\hbar\omega$ and wire radius R. Note the logarithmic scale for the magtnitude of the effect. (a) Dependence of the SPIDEr emf per unit SPP power $\mathscr{E}/\mathscr{P}$ on wire radius and frequency. The black broken curve indicates the parameters at which SPP pressure is equal to striction. The magnitude of the effect is denoted by the color-coding bar. (b) Dependence of SPIDEr magnitude $\mathscr{E}$ on wire radius R per unit power of the SPP wave (solid red curve). The contributions of the pressure and striction to the total magnitude of SPIDEr are shown by the dashed curves. (c) Dependence of SPIDEr magnitude per unit power $\mathscr{E}/\mathscr{P}$ on frequency ω for $R = 5\,\text{nm}$. (d) Maximum power that a wire can tolerate $\mathscr{P}_m$ as a function of wire radius R for different frequencies ω. (e) The maximum SPIDEr rectified field E_{mR} (for the maximum tolerable power $\mathscr{P}_m$) as a function of frequency for three wire radii R = 5, 30, and 100 nm. (f) The maximum SPIDEr rectified field E_{mR} (for the maximum tolerable power $\mathscr{P}_m$) as a function of the wire radius R for frequency $\hbar\omega = 1.55\,\text{eV}$.

the maximum achievable rectified field E_{mR} (at the propagating SPP power of $\mathscr{P}_m$) in Figure 5.2(e), (f). As we see from panel (e), the spectral dependence of the SPIDEr rectified THz field is very similar for all wire sizes, but the magnitude of this field is much greater for the 5 nm wire: $E_{mR} \sim 10^5 - 10^6$ V/cm. The nanolocalized THz fields of such a magnitude will excite a wealth of nonlinear THz responses at the nanoscale.

5.4 SPIDEr as a Femtosecond SPP Detector

Now let us consider dynamics of the emf response to SPP pulses that differ in duration τ with respect to the SPP pulse dissipation time t_p. The latter is displayed in Figure 5.3(a) as a function of the frequency ω. As we can see time t_p is in the range from 10 to 150 fs. The temporal dependencies of the emf in comparison with the power $\mathscr{P}$ of the SPP pulses for various pulse durations are illustrated in Figure 5.3(b)-(d). For a relatively long pulse ($\tau = 1\text{ps} >> t_p$) shown in Figure 5.3(b), the shape of the emf $\mathscr{E}(t)$ repeats that of the power $\mathscr{P}(t)$. This relatively long, picosecond response, nevertheless, corresponds to a 1 THz bandwidth for this nanowire used as a nanoscale photodetector. Note that the amplitude of the emf is very large, ~ 10 V.

For a much shorter, $\tau = 40\,\text{fs}$, SPP pulse and the same 5 nm wire, as shown in Figure 5.3(c), there is a small broadening and delay of the voltaic response (emf) $\mathscr{E}(t)$ with respect to the excitation SPP pulse $\mathscr{P}(t)$. This broadening is due to the pressure force that decays exponentially for long times, as Eq. (5.4) suggests, and the broken blue line in the figure indicates. However, under the conditions considered, this delay and broadening are not large. The frequency-response bandwidth of this wire as an SPP photodetector on the nanoscale is very

large, ~ 20 THz, which is characteristic of the extreme nanoplasmonic confinement. The amplitude of the SPIDEr emf is also very large, $\mathscr{E} \sim 10\,\mathrm{V}$.

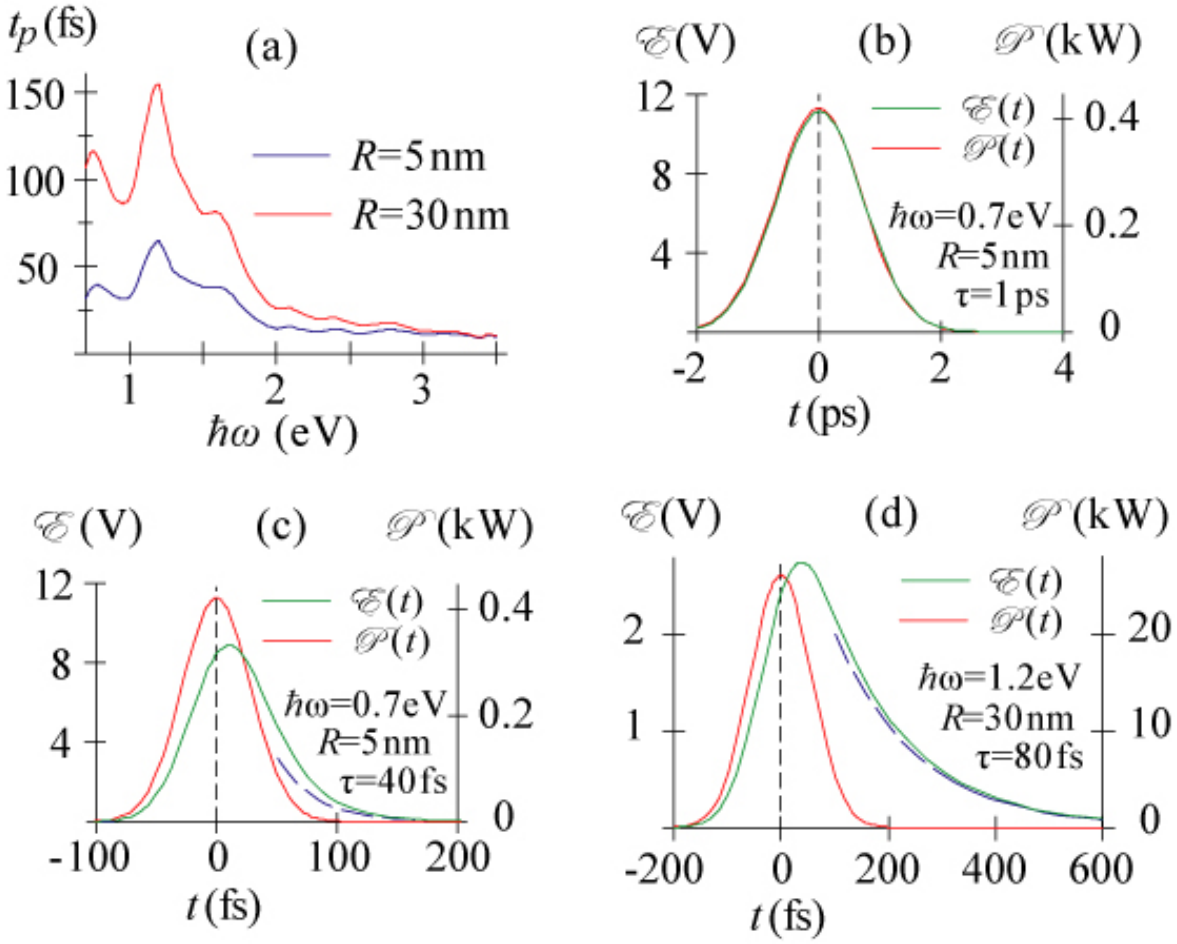

Figure 5.3. (color online) SPIDEr created by ultrashort SPP pulses: fast femtosecond emf response. (a) The dependence of the SPP lifetime $t_p = l_p / v_g$ on the frequency $\hbar\omega$ for $R = 5\,\mathrm{nm}$ and $R = 30\,\mathrm{nm}$. (b) The time dependence of the emf $\mathscr{E}(t)$ (green line, left scale) and input power $\mathscr{P}(t)$ (red line, right scale). The pulse duration is $\tau = 1\,\mathrm{ps} >> t_p \approx 30\,\mathrm{fs}$ and the emf closely follows the SPP pulse dynamics. (c) The same for much shorter pulse with $\tau = 40\,\mathrm{fs}$. The pressure-induced emf leads to a small broadening in the emf dynamics (green line). The limiting exponential decay is outlined by the broken blue line. (d) Emf induced by the short pulse in nanowire with $R = 30\,\mathrm{nm}$ with frequency $\hbar\omega = 1.2\ \mathrm{eV}$. The emf response is broadened, since $\tau = 80\,\mathrm{fs}$, while $t_p = 150\ \mathrm{fs}$.

For a much thicker nanowire of $R = 30\,\mathrm{nm}$ (weak plasmonic confinement case) and $\hbar\omega = 1.2\ \mathrm{eV}$, illustrated in Fig. 3 (d), the SPP decay time becomes much longer ($t_p = 150\ \mathrm{fs}$).

This leads to a very significant delay and temporal broadening of the emf response with a pronounced exponential part due to the pressure forces shown by the broken blue line. This behavior is due to the much longer SPP lifetimes for the weak confinement where a significant fraction of the SPP energy propagates in the dielectric (vacuum). Nevertheless the emf response bandwidth is still very large, on the order of 5 THz, and its amplitude is also very large, $\mathscr{E} \geq 1$ V.

5.5 Conclusion

In conclusion, the ultrafast giant SPIDEr in metal nanowires excited by ultrashort SPP pulses was predicted in paper [118] to generate a gigantic emf up to $\sim$ 10 V for the SPP waves of realistic and tolerable amplitudes. The SPIDEr enhancement is mostly nonresonant, due to nanoplasmonic confinement of the SPP fields, which leads to higher gradients of the fields and their higher magnitudes. Because of its nonresonant nature, the SPIDEr is an extremely fast effect: the frequency bandwidth of the generated THz fields is realistically 5-20 THz. Due to the high longitudinal localization of the SPP waves in the case of the strong nanoplasmonic confinement, the SPIDEr generates very high local THz electric fields at the metal surface, $E_R \sim 10^5 - 10^6$ V/cm. Such fields are capable of inducing strongly nonlinear responses, including dissociation of molecules. Among possible applications of the giant SPIDEr are rectification and detection of the nanoscale femtosecond optical fields, coupling of the nanoplasmonic elements to semiconductor devices, nonlinear THz spectroscopy on the nanoscale of chemical and biological nanoobjects for biomedicine, etc.

References

1. Landau, L.D. and E.M. Lifshitz, *Theoretical Physics. The Theory of Field*. Vol. 2. 1988, Moscow: Nauka.

2. Jackson, J.D., *Classical Electrodynamics*. 3rd ed. 1998, New York: Wiley.

3. Stratton, J.A., *Electromagnetic Theory*. 1941, New York and London: McGraw-Hill.

4. Stockman, M.I., L.N. Pandey, L.S. Muratov, and T.F. George, *Giant Fluctuations of Local Optical Fields in Fractal Clusters.* Physical Review Letters, 1994. **72**(15): p. 2486-2489.

5. Stockman, M.I., *Giant Attosecond Fluctuations of Local Optical Fields in Disordered Nanostructured Media.* Physical Review B, 2000. **62**(15): p. 10494-10497.

6. Landau, L.D. and E.M. Lifshitz, *Theoretical Physics. Electrodynamics of Continuous Media*. Vol. 8. 2005, Moscow: Nauka.

7. Lifshitz, E.M. and L.P. Pitaevskii, *Theoretical Physics. Physical Kinetics.* Vol. 10. 1979, Moscow: Nauka.

8. Larkin, I.A. and M.I. Stockman, *Imperfect Perfect Lens.* Nano Letters, 2005. **5**(2): p. 339-343.

9. Aizpurua, J. and A. Rivacoba, *Nonlocal Effects in the Plasmons of Nanowires and Nanocavities Excited by Fast Electron Beams.* Physical Review B, 2008. **78**(3): p. 035404-14.

10. Chapuis, P.-O., S. Volz, C. Henkel, K. Joulain, and J.-J. Greffet, *Effects of Spatial Dispersion in Near-Field Radiative Heat Transfer between Two Parallel Metallic Surfaces.* Physical Review B, 2008. **77**(3): p. 035431-9.

11. Fuchs, R. and R.G. Barrera, *Dynamical Response of a Dipole near the Surface of a Nonlocal Metal.* Physical Review B, 1981. **24**(6): p. 2940.

12. Born, M. and E. Wolf, *Principles of Optics*. 1999, Cambridge: University Press.

13. Johnson, P.B. and R.W. Christy, *Optical-Constants of Noble Metals.* Physical Review B, 1972. **6**(12): p. 4370-4379.

14. Bergman, D.J. and Y. Imry, *Critical Behavior of the Complex Dielectric Constant near the Percolation Threshold of a Heterogeneous Material.* Physical Review Letters, 1977. **39**(19): p. 1222.

15. Bergman, D.J., *The Dielectric Constant of a Composite Material-a Problem in Classical Physics.* Physics Reports, 1978. **43**(9): p. 377-407.

16. Stockman, M.I., S.V. Faleev, and D.J. Bergman, *Localization Versus Delocalization of Surface Plasmons in Nanosystems: Can One State Have Both Characteristics?* Physical Review Letters, 2001. **87**(16): p. 167401.

17. Stockman, M.I., S.V. Faleev, and D.J. Bergman, *Coherent Control of Femtosecond Energy Localization in Nanosystems.* Physical Review Letters, 2002. **88**(6): p. 067402.

18. Aeschlimann, M., M. Bauer, D. Bayer, T. Brixner, F.J. Garcia de Abajo, W. Pfeiffer, M. Rohmer, C. Spindler, and F. Steeb, *Adaptive Subwavelength Control of Nano-Optical Fields.* Nature, 2007. **446**(7133): p. 301-304.

19. Stockman, M., *Electromagnetic Theory of SERS*, in Topics in Applied Physics, eds. K. Kneipp, M. Moskovits, and H. Kneipp. Vol 103. 2006, Berlin Heidelberg New York: Springer.

20. Bergman, D.J. and M.I. Stockman, *Surface Plasmon Amplification by Stimulated Emission of Radiation: Quantum Generation of Coherent Surface Plasmons in Nanosystems.* Physical Review Letters, 2003. **90**(2): p. 027402.

21. Noginov, M.A., G. Zhu, A.M. Belgrave, R. Bakker, V.M. Shalaev, E.E. Narimanov, S. Stout, E. Herz, T. Suteewong, and U. Wiesner, *Demonstration of a Spaser-Based Nanolaser.* Nature, 2009. **460**(7259): p. 1110-1112.

22. *Focus on Plasmonics*, in *New Journal of Physics*, S. Bozhevolnyi and F. García-Vidal, Editors. 2008.

23. Willets, K.A. and R.P. Van Duyne, *Localized Surface Plasmon Resonance Spectroscopy and Sensing.* Annual Review of Physical Chemistry, 2007. **58**(1): p. 267-297.

24. *Near-Field Optics and Surface Plasmon Polaritons*. Topics in Applied Physics, ed. S. Kawata. Vol. 81. 2001, Berlin Heidelberg New York: Springer-Verlag.

25. Maier, S., *Plasmonics: Fundamentals and Applications*. 2007: Springer.

26. Novotny, L. and B. Hecht, *Principles of Nano-Optics*. 2006, Cambridge, New York: Cambridge University Press.

27. Bosbach, J., C. Hendrich, F. Stietz, T. Vartanyan, and F. Träger, *Ultrafast Dephasing of Surface Plasmon Excitation in Silver Nanoparticles: Influence of Particle Size, Shape, and Chemical Surrounding.* Physical Review Letters, 2002. **89**(25): p. 257404.

28. Li, J., H. Iu, D.Y. Lei, J.T.K. Wan, J.B. Xu, H.P. Ho, M.Y. Waye, and H.C. Ong, *Dependence of Surface Plasmon Lifetimes on the Hole Size in Two-Dimensional Metallic Arrays.* Applied Physics Letters, 2009. **94**(18): p. 183112-3.

29. Sönnichsen, C., T. Franzl, T. Wilk, G. von Plessen, J. Feldmann, O. Wilson, and P. Mulvaney, *Drastic Reduction of Plasmon Damping in Gold Nanorods.* Physical Review Letters, 2002. **88**(7): p. 077402.

30. Little, J.W., T.A. Callcott, T.L. Ferrell, and E.T. Arakawa, *Surface-Plasmon Radiation from Ellipsoidal Silver Spheroids.* Physical Review B, 1984. **29**(4): p. 1606.

31. Dulkeith, E., T. Niedereichholz, T.A. Klar, J. Feldmann, G. von Plessen, D.I. Gittins, K.S. Mayya, and F. Caruso, *Plasmon Emission in Photoexcited Gold Nanoparticles.* Physical Review B, 2004. **70**(20): p. 205424.

32. Kokkinakis, T. and K. Alexopoulos, *Observation of Radiative Decay of Surface Plasmons in Small Silver Particles.* Physical Review Letters, 1972. **28**(25): p. 1632.

33. Fleischmann, M., P.J. Hendra, and A.J. McQuillan, *Raman Spectra of Pyridine Adsorbed at a Silver Electrode.* Chemical Physics Letters, 1974. **26**(2): p. 163-166.

34. Jeanmaire, D.L. and R.P. Van Duyne, *Surface Raman Spectroelectrochemistry: Part I. Heterocyclic, Aromatic, and Aliphatic Amines Adsorbed on the Anodized Silver Electrode.* Journal of Electroanalytical Chemistry, 1977. **84**(1): p. 1-20.

35. Albrecht, M.G. and J.A. Creighton, *Anomalously Intense Raman Spectra of Pyridine at a Silver Electrode.* Journal of the American Chemical Society, 2002. **99**(15): p. 5215-5217.

36. Kneipp, K., Y. Wang, H. Kneipp, L.T. Perelman, I. Itzkan, R.R. Dasari, and M.S. Feld, *Single Molecule Detection Using Surface-Enhanced Raman Scattering (SERS).* Physical Review Letters, 1997. **78**(9): p. 1667.

37. Hartschuh, A., H.N. Pedrosa, L. Novotny, and T.D. Krauss, *Simultaneous Fluorescence and Raman Scattering from Single Carbon Nanotubes.* Science, 2003. **301**(5638): p. 1354-1356.

38. Lakowicz, J.R., *Radiative Decay Engineering: Biophysical and Biomedical Applications.* Analytical Biochemistry, 2001. **298**(1): p. 1-24.

39. Shimizu, K.T., W.K. Woo, B.R. Fisher, H.J. Eisler, and M.G. Bawendi, *Surface-Enhanced Emission from Single Semiconductor Nanocrystals.* Physical Review Letters, 2002. **89**(11): p. 117401.

40. Gerton, J.M., L.A. Wade, G.A. Lessard, Z. Ma, and S.R. Quake, *Tip-Enhanced Fluorescence Microscopy at 10 Nanometer Resolution.* Physical Review Letters, 2004. **93**(18): p. 180801.

41. Kuhn, S., U. Hakanson, L. Rogobete, and V. Sandoghdar, *Enhancement of Single-Molecule Fluorescence Using a Gold Nanoparticle as an Optical Nanoantenna.* Physical Review Letters, 2006. **97**(1): p. 017402-4.

42. Novotny, L. and S.J. Stranick, *Near-Field Optical Microscopy and Spectroscopy with Pointed Probes.* Annual Review of Physical Chemistry, 2006. **57**(1): p. 303-331.

43. Dulkeith, E., M. Ringler, T.A. Klar, J. Feldmann, A. Munoz Javier, and W.J. Parak, *Gold Nanoparticles Quench Fluorescence by Phase Induced Radiative Rate Suppression.* Nano Letters, 2005. **5**(4): p. 585-589.

44. Ichimura, T., N. Hayazawa, M. Hashimoto, Y. Inouye, and S. Kawata, *Tip-Enhanced Coherent Anti-Stokes Raman Scattering for Vibrational Nanoimaging.* Physical Review Letters, 2004. **92**(22): p. 220801.

45. Kneipp, J., H. Kneipp, and K. Kneipp, *Two-Photon Vibrational Spectroscopy for Biosciences Based on Surface-Enhanced Hyper-Raman Scattering.* Proceedings of the National Academy of Sciences, 2006. **103**(46): p. 17149-17153.

46. Durach, M., A. Rusina, V.I. Klimov, and M.I. Stockman, *Nanoplasmonic Renormalization and Enhancement of Coulomb Interactions.* New Journal of Physics, 2008. **10**: p. 105011.

47. West, J.L. and N.J. Halas, *Engineered Nanomaterials for Biophotonics Applications: Improving Sensing, Imaging, and Therapeutics.* Annual Review of Biomedical Engineering, 2003. **5**(1): p. 285-292.

48. Achermann, M., M.A. Petruska, S. Kos, D.L. Smith, D.D. Koleske, and V.I. Klimov, *Energy-Transfer Pumping of Semiconductor Nanocrystals Using an Epitaxial Quantum Well.* Nature, 2004. **429**(6992): p. 642-646.

49. Gradstein, I.S. and I.M. Ryzhik, *Tables of Integrals, Series and Products.* 1963, Moscow: Fizmatgiz.

50. Förster, T., *Zwischenmolekulare Energiewanderung und Fluoreszenz.* Annalen der Physik, 1948. **437**(1-2): p. 55-75.

51. Dexter, D.L., *A Theory of Sensitized Luminescence in Solids.* The Journal of Chemical Physics, 1953. **21**(5): p. 836-850.

52. Hua, X.M., J.I. Gersten, and A. Nitzan, *Theory of Energy Transfer between Molecules near Solid State Particles.* The Journal of Chemical Physics, 1985. **83**(7): p. 3650-3659.

53. Govorov, A.O., J. Lee, and N.A. Kotov, *Theory of Plasmon-Enhanced Förster Energy Transfer in Optically-Excited Semiconductor and Metal Nanoparticles.* Physical Review B, 2007. **76**(12): p. 125308-16.

54. Andrew, P. and W.L. Barnes, *Energy Transfer across a Metal Film Mediated by Surface Plasmon Polaritons.* Science, 2004. **306**(5698): p. 1002-1005.

55. Kagan, C.R., C.B. Murray, M. Nirmal, and M.G. Bawendi, *Electronic Energy Transfer in CdSe Quantum Dot Solids.* Physical Review Letters, 1996. **76**(9): p. 1517.

56. Crooker, S.A., J.A. Hollingsworth, S. Tretiak, and V.I. Klimov, *Spectrally Resolved Dynamics of Energy Transfer in Quantum-Dot Assemblies: Towards Engineered Energy Flows in Artificial Materials.* Physical Review Letters, 2002. **89**(18): p. 186802.

57. Achermann, M., M.A. Petruska, S.A. Crooker, and V.I. Klimov, *Picosecond Energy Transfer in Quantum Dot Langmuir-Blodgett Nanoassemblies.* Journal of Physical Chemistry B, 2003. **107**(50): p. 13782-13787.

58. Dai, J., F. Cajko, I. Tsukerman, and M.I. Stockman, *Electrodynamic Effects in Plasmonic Nanolenses.* Physical Review B, 2008. **77**(11): p. 115419.

59. Merlin, R., *Metamaterials and the Landau-Lifshitz Permeability Argument: Large Permittivity Begets High-Frequency Magnetism.* Proceedings of the National Academy of Sciences of the United States of America, 2009. **106**(6): p. 1693-1698.

60. Teperik, T.V., V.V. Popov, and F.J. García de Abajo, *Radiative Decay of Plasmons in a Metallic Nanoshell.* Physical Review B, 2004. **69**(15): p. 155402.

61. Bergman, D.J. and D. Stroud, *Theory of Resonances in the Electromagnetic Scattering by Macroscopic Bodies.* Physical Review B, 1980. **22**(8): p. 3527.

62. Evra, U. and D.J. Bergman. *Lifetime of Nanoplasmonic States*. in *Plasmonics: Nanoimaging, Nanofabrication, and their Applications II*. 2006. San Diego: SPIE.

63. Landau, L.D. and E.M. Lifshitz, *Theoretical Physics. Quantum Mechanics. Nonrelativistic Theory*. Vol. 3. 1989, Moscow: Nauka.

64. Ching, E.S.C., P.T. Leung, A. Maassen van den Brink, W.M. Suen, S.S. Tong, and K. Young, *Quasinormal-Mode Expansion for Waves in Open Systems.* Reviews of Modern Physics, 1998. **70**(4): p. 1545.

65. Stockman, M.I., *(Unpublished).*

66. *Plasmonic Nanoguides and Circuits*, ed. S.I. Bozhevolnyi. 2008, Singapore: Pan Stanford Publishing.

67. Moreland, J., A. Adams, and P.K. Hansma, *Efficiency of Light Emission from Surface Plasmons.* Physical Review B, 1982. **25**(4): p. 2297.

68. Hutley, M.C. and D. Maystre, *The Total Absorption of Light by a Diffraction Grating.* Optics Communications, 1976. **19**(3): p. 431-436.

69. Devaux, E., T.W. Ebbesen, J.-C. Weeber, and A. Dereux, *Launching and Decoupling Surface Plasmons Via Micro-Gratings.* Applied Physics Letters, 2003. **83**(24): p. 4936-4938.

70. Schröter, U. and D. Heitmann, *Grating Couplers for Surface Plasmons Excited on Thin Metal Films in the Kretschmann-Raether Configuration.* Physical Review B, 1999. **60**(7): p. 4992.

71. Worthing, P.T. and W.L. Barnes, *Efficient Coupling of Surface Plasmon Polaritons to Radiation Using a Bi-Grating.* Applied Physics Letters, 2001. **79**(19): p. 3035-3037.

72. Renger, J., S. Grafstrom, and L.M. Eng, *Direct Excitation of Surface Plasmon Polaritons in Nanopatterned Metal Surfaces and Thin Films.* Physical Review B, 2007. **76**(4): p. 045431-7.

73. Wood, R.W., *On a Remarkable Case of Uneven Distribution of Light in a Diffraction Grating Spectrum.* Proceedings of the Physical Society of London, 1902. **18**(1): p. 269-275.

74. Ritchie, R.H., E.T. Arakawa, J.J. Cowan, and R.N. Hamm, *Surface-Plasmon Resonance Effect in Grating Diffraction.* Physical Review Letters, 1968. **21**(22): p. 1530.

75. Hibbins, A.P., B.R. Evans, and J.R. Sambles, *Experimental Verification of Designer Surface Plasmons.* Science, 2005. **308**(5722): p. 670-672.

76. Pendry, J.B., L. Martin-Moreno, and F.J. Garcia-Vidal, *Mimicking Surface Plasmons with Structured Surfaces.* Science, 2004. **305**(5685): p. 847-848.

77. Garcia-Vidal, F.J., L. Martin-Moreno, and J.B. Pendry, *Surfaces with Holes in Them: New Plasmonic Metamaterials.* Journal of Optics A: Pure and Applied Optics, 2005(2): p. S97.

78. Martín-Moreno, L., F.J. García-Vidal, H.J. Lezec, K.M. Pellerin, T. Thio, J.B. Pendry, and T.W. Ebbesen, *Theory of Extraordinary Optical Transmission through Subwavelength Hole Arrays.* Physical Review Letters, 2001. **86**(6): p. 1114.

79. Lezec, H.J., A. Degiron, E. Devaux, R.A. Linke, L. Martin-Moreno, F.J. Garcia-Vidal, and T.W. Ebbesen, *Beaming Light from a Subwavelength Aperture.* Science, 2002. **297**(5582): p. 820-822.

80. Lopez-Tejeira, F., S.G. Rodrigo, L. Martin-Moreno, F.J. Garcia-Vidal, E. Devaux, J. Dintinger, T.W. Ebbesen, J.R. Krenn, I.P. Radko, S.I. Bozhevolnyi, M.U. Gonzalez, J.C. Weeber, and A. Dereux, *Modulation of Surface Plasmon Coupling-in by One-Dimensional Surface Corrugation.* New Journal of Physics, 2008. **10**(3): p. 033035.

81. Genet, C. and T.W. Ebbesen, *Light in Tiny Holes.* Nature, 2007. **445**(7123): p. 39-46.

82. Otto, A., *Excitation of Nonradiative Surface Plasma Waves in Silver by the Method of Frustrated Total Reflection.* Zeitschrift für Physik A Hadrons and Nuclei, 1968. **216**(4): p. 398-410.

83. Kretschmann, E. and H. Raether, *Radiative Decay of Nonradiative Surface Plasmons Excited by Light* Zeitschrift fuer Naturforschung, Teil A: Astrophysik, Physik und Physikalische Chemie, 1968. **23**(12): p. 2135-6.

84. Lockyear, M.J., A.P. Hibbins, and J.R. Sambles, *Microwave Surface-Plasmon-Like Modes on Thin Metamaterials.* Physical Review Letters, 2009. **102**(7): p. 073901-4.

85. Charbonneau, R. and P. Berini, *Broadside Coupling to Long-Range Surface Plasmons in Metal Stripes Using Prisms, Particles, and an Atomic Force Microscope Probe.* Review of Scientific Instruments, 2008. **79**(7): p. 073106-9.

86. Krenn, J.R. and J.C. Weeber, *Surface Plasmon Polaritons in Metal Stripes and Wires.* Philosophical Transactions: Mathematical, Physical and Engineering Sciences, 2004. **362**(1817): p. 739-756.

87. Knight, M.W., N.K. Grady, R. Bardhan, F. Hao, P. Nordlander, and N.J. Halas, *Nanoparticle-Mediated Coupling of Light into a Nanowire.* Nano Letters, 2007. **7**(8): p. 2346-2350.

88. Ritchie, R.H., *Plasma Losses by Fast Electrons in Thin Films.* Physical Review, 1957. **106**(5): p. 874.

89. Cai, W., R. Sainidou, J. Xu, A. Polman, and F.J. García de Abajo, *Efficient Generation of Propagating Plasmons by Electron Beams.* Nano Letters, 2009. **9**(3): p. 1176-1181.

90. Dickson, R.M. and L.A. Lyon, *Unidirectional Plasmon Propagation in Metallic Nanowires.* The Journal of Physical Chemistry B, 2000. **104**(26): p. 6095-6098.

91. Ditlbacher, H., A. Hohenau, D. Wagner, U. Kreibig, M. Rogers, F. Hofer, F.R. Aussenegg, and J.R. Krenn, *Silver Nanowires as Surface Plasmon Resonators.* Physical Review Letters, 2005. **95**(25): p. 257403.

92. Leosson, K., T. Nikolajsen, A. Boltasseva, and S.I. Bozhevolnyi, *Long-Range Surface Plasmon Polariton Nanowire Waveguides for Device Applications.* Optics Express, 2006. **14**(1): p. 314-319.

93. Chang, D.E., A.S. Sorensen, P.R. Hemmer, and M.D. Lukin, *Quantum Optics with Surface Plasmons.* Physical Review Letters, 2006. **97**(5): p. 053002-4.

94. Akimov, A.V., A. Mukherjee, C.L. Yu, D.E. Chang, A.S. Zibrov, P.R. Hemmer, H. Park, and M.D. Lukin, *Generation of Single Optical Plasmons in Metallic Nanowires Coupled to Quantum Dots.* Nature, 2007. **450**(7168): p. 402-406.

95. Stockman, M.I., *Nanofocusing of Optical Energy in Tapered Plasmonic Waveguides.* Physical Review Letters, 2004. **93**(13): p. 137404.

96. Verhagen, E., M. Spasenovic, A. Polman, and L. Kuipers, *Nanowire Plasmon Excitation by Adiabatic Mode Transformation.* Physical Review Letters, 2009. **102**(20): p. 203904-4.

97. *The Wolfram Functions Site*. Available from: http://functions.wolfram.com/.

98. MacDonald, K.F., Z.L. Samson, M.I. Stockman, and N.I. Zheludev, *Ultrafast Active Plasmonics.* Nat Photon, 2009. **3**(1): p. 55-58.

99. Minogin, V.G. and V.S. Letokhov, *Laser Light Pressure on Atoms*. 1986, Moscow: Nauka.

100. Maxwell, J.C., *A Treatise on Electricity and Magnetism*. 1873, Claredon Press.

101. Lebedew, P., *Untersuchungen über die Druckkräfte des Lichtes.* Annalen der Physik, 1901. **311**(11): p. 433-458.

102. Einstein, A., *Über Einen die Erzeugung und Verwandlung des Lichtes betreffenden heuristischen Gesichtspunkt.* Annalen der Physik, 1905. **322**(6): p. 132-148.

103. Planck, M., *Über das Gesetz der Energieverteilung im Normalspectrum.* Annalen der Physik, 1901. **309**(3): p. 553-563.

104. Einstein, A. and W. Ritz, *Zum gegenwärtigen Stand des Strahlungsproblems.* Physikalische Zeitschrift, 1909. **10**: p. 185-193.

105. Compton, A.H., *The Corpuscular Properties of Light.* Naturwissenschaften, 1929. **17**(26): p. 507-515.

106. Frisch, R., *Experimenteller Nachweis des Einsteinschen Strahlungsrückstoßes.* Zeitschrift für Physik A Hadrons and Nuclei, 1933. **86**(1): p. 42-48.

107. Ashkin, A., *Acceleration and Trapping of Particles by Radiation Pressure.* Physical Review Letters, 1970. **24**(4): p. 156.

108. Ashkin, A., *Trapping of Atoms by Resonance Radiation Pressure.* Physical Review Letters, 1978. **40**(12): p. 729.

109. Letokhov, V.S., V.G. Minogin, and B.D. Pavlik, *Cooling and Capture of Atoms and Molecules by a Resonant Light Field.* Soviet Physics - JETP, 1977. **45**(4): p. 698-705.

110. Ashkin, A. and J.M. Dziedzic, *Optical Trapping and Manipulation of Viruses and Bacteria.* Science, 1987. **235**(4795): p. 1517-1520.

111. Novotny, L., R.X. Bian, and X.S. Xie, *Theory of Nanometric Optical Tweezers.* Physical Review Letters, 1997. **79**(4): p. 645.

112. Righini, M., G. Volpe, C. Girard, D. Petrov, and R. Quidant, *Surface Plasmon Optical Tweezers: Tunable Optical Manipulation in the Femtonewton Range.* Physical Review Letters, 2008. **100**(18): p. 186804-4.

113. Hänsch, T.W. and A.L. Schawlow, *Cooling of Gases by Laser Radiation.* Optics Communications, 1975. **13**(1): p. 68-69.

114. Danishevskii, A.M., A.A. Kastalskii, S.M. Ryvkin, and I.D. Yaroshetskii, *Dragging of Free Carriers by Photons in Direct Interband Transitions in Semiconductors.* Sov. Phys. JETP, 1970. **31**: p. 292.

115. Gibson, A.F., M.F. Kimmitt, and A.C. Walker, *Photon Drag in Germanium.* Applied Physics Letters, 1970. **17**(2): p. 75-77.

116. Ganichev, S. and W. Prettl, *Intense Terahertz Excitation of Semiconductors*. 2006, Oxford, New York: Oxford University Press.

117. Shimizu, Y. and H. Sasada, *Mechanical Force in Laser Cooling and Trapping.* American Journal of Physics, 1998. **66**(11): p. 960-967.

118. Durach, M., A. Rusina, and M.I. Stockman, *Giant Surface-Plasmon-Induced Drag Effect in Metal Nanowires.* Physical Review Letters, 2009. **103**(18): p. 186801-4.

119. Volpe, G., R. Quidant, G. Badenes, and D. Petrov, *Surface Plasmon Radiation Forces.* Physical Review Letters, 2006. **96**(23): p. 238101-4.

120. Kalmykov, S., O. Polomarov, D. Korobkin, J. Otwinowski, J. Power, and G. Shvets, *Novel Techniques of Laser Acceleration: From Structures to Plasmas.* Royal Society of London Transactions Series A, 2006. **364**: p. 725.

121. Vengurlekar, A.S. and T. Ishihara, *Surface Plasmon Enhanced Photon Drag in Metal Films.* Applied Physics Letters, 2005. **87**(9): p. 091118-3.

122. Hatano, T., B. Nishikawa, M. Iwanaga, and T. Ishihara, *Optical Rectification Effect in 1d Metallic Photonic Crystal Slabs with Asymmetric Unit Cell.* Optics Express, 2008. **16**(11): p. 8236-8241.

123. Sell, A., A. Leitenstorfer, and R. Huber, *Phase-Locked Generation and Field-Resolved Detection of Widely Tunable Terahertz Pulses with Amplitudes Exceeding 100 MV/cm.* Optics Letters, 2008. **33**(23): p. 2767-2769.

124. Leinss, S., T. Kampfrath, K. v.Volkmann, M. Wolf, J.T. Steiner, M. Kira, S.W. Koch, A. Leitenstorfer, and R. Huber, *Terahertz Coherent Control of Optically Dark Paraexcitons in Cu_2O.* Physical Review Letters, 2008. **101**(24): p. 246401-4.

125. Gault, B., F. Vurpillot, A. Bostel, A. Menand, and B. Deconihout, *Estimation of the Tip Field Enhancement on a Field Emitter under Laser Illumination.* Applied Physics Letters, 2005. **86**(9): p. 094101-3.

126. Sha, G., A. Cerezo, and G.D.W. Smith, *Field Evaporation Behavior During Irradiation with Picosecond Laser Pulses.* Applied Physics Letters, 2008. **92**(4): p. 043503-3.